

Stochastic accretion of planetesimals on to white dwarfs: constraints on the mass distribution of accreted material from atmospheric pollution

M. C. Wyatt, J. Farihi, J. E. Pringle, A. Bonsor

▶ **To cite this version:**

M. C. Wyatt, J. Farihi, J. E. Pringle, A. Bonsor. Stochastic accretion of planetesimals on to white dwarfs: constraints on the mass distribution of accreted material from atmospheric pollution. Monthly Notices of the Royal Astronomical Society, 2014, 439, pp.3371-3391. 10.1093/mnras/stu183 . insu-03618586

HAL Id: insu-03618586
https://insu.hal.science/insu-03618586

Submitted on 24 Mar 2022

HAL is a multi-disciplinary open access archive for the deposit and dissemination of scientific research documents, whether they are published or not. The documents may come from teaching and research institutions in France or abroad, or from public or private research centers.

L'archive ouverte pluridisciplinaire **HAL**, est destinée au dépôt et à la diffusion de documents scientifiques de niveau recherche, publiés ou non, émanant des établissements d'enseignement et de recherche français ou étrangers, des laboratoires publics ou privés.



Distributed under a Creative Commons Attribution 4.0 International License

Monthly Notices
of the
ROYAL ASTRONOMICAL SOCIETY

MNRAS **439,** 3371–3391 (2014)
Advance Access publication 2014 February 28

doi:10.1093/mnras/stu183

Stochastic accretion of planetesimals on to white dwarfs: constraints on the mass distribution of accreted material from atmospheric pollution

M. C. Wyatt,[1]★ J. Farihi,[1]† J. E. Pringle[1] and A. Bonsor[2,3]

[1]*Institute of Astronomy, University of Cambridge, Madingley Road, Cambridge CB3 0HA, UK*
[2]*Institut de Planétologie et d'Astrophysique de Grenoble, Université Joseph Fourier, CNRS, BP 53, F-38041 Grenoble, France*
[3]*H.H. Wills Physics Laboratory, University of Bristol, Tyndall Avenue, Bristol BS8 1TL, UK*

Accepted 2014 January 22. Received 2014 January 10; in original form 2013 October 8

Downloaded from https://academic.oup.com/mnras/article/439/4/3371/1151716 by guest on 24 March 2022

ABSTRACT

This paper explores how the stochastic accretion of planetesimals on to white dwarfs would be manifested in observations of their atmospheric pollution. Archival observations of pollution levels for unbiased samples of DA and non-DA white dwarfs are used to derive the distribution of inferred accretion rates, confirming that rates become systematically lower as sinking time (assumed here to be dominated by gravitational settling) is decreased, with no discernable dependence on cooling age. The accretion rates expected from planetesimals that are all the same mass (i.e., a mono-mass distribution) are explored both analytically and using a Monte Carlo model, quantifying how measured accretion rates inevitably depend on sinking time, since different sinking times probe different times since the last accretion event. However, that dependence is so dramatic that a mono-mass distribution can be excluded within the context of this model. Consideration of accretion from a broad distribution of planetesimal masses uncovers an important conceptual difference: accretion is continuous (rather than stochastic) for planetesimals below a certain mass, and the accretion of such planetesimals determines the rate typically inferred from observations; smaller planetesimals dominate the rates for shorter sinking times. A reasonable fit to the observationally inferred accretion rate distributions is found with model parameters consistent with a collisionally evolved mass distribution up to Pluto-mass, and an underlying accretion rate distribution consistent with that expected from descendants of debris discs of main-sequence A stars. With these parameters, while both DA and non-DA white dwarfs accrete from the same broad planetesimal distribution, this model predicts that the pollution seen in DAs is dominated by the continuous accretion of <35 km objects, and that in non-DAs by >35 km objects (though the dominant size varies between stars by around an order of magnitude from this reference value). Furthermore, observations that characterize the dependence of inferred accretion rates on sinking time and cooling age (including a consideration of the effect of thermohaline convection on models used to derive those rates), and the decadal variability of DA accretion signatures, will improve constraints on the mass distribution of accreted material and the lifetime of the disc through which it is accreted.

Key words: circumstellar matter – planetary systems – white dwarfs.

1 INTRODUCTION

Our understanding of the planetary systems around main-sequence Sun-like stars has grown enormously in the past few years. Not only do we know about planets like Jupiter orbiting 0.05–5 au from their stars, but a new population of low-mass planets (2–20 times the mass of Earth) orbiting within 1 au has been found in transit and radial velocity surveys, as well a more distant 8–200 au population of giant planets found in imaging surveys (Udry & Santos 2007; Marois et al. 2008). Our understanding of the debris discs, i.e. belts of planetesimals and dust, orbiting main-sequence stars has also grown rapidly; surveys show that >50 per cent of early-type stars

★ E-mail: wyatt@ast.cam.ac.uk
† STFC Ernest Rutherford Fellow.

© 2014 The Authors
Published by Oxford University Press on behalf of the Royal Astronomical Society

host debris (Wyatt 2008). Most of this debris lies $\gg$10 au in regions analogous to the Solar system's Kuiper belt, but a few per cent of stars exhibit dust at $\sim$1 au that may originate in an asteroid belt analogue.

Much less is known about the planetary systems and debris of post-main-sequence stars, though these should be direct descendants of the main-sequence population. Several post-main-sequence planetary systems are now known (e.g., Johnson et al. 2011), but the debris discs of post-main-sequence stars have remained elusive (though there are examples around sub-giants, e.g., Bonsor et al. 2013). The closest to a counterpart of the Kuiper belt-like discs found around main-sequence stars may be the 30–150 au disc at the centre of the Helix nebula (Su et al. 2007) and a few others like it (Chu et al. 2011; Bilikova et al. 2012). However, a more ubiquitous phenomenon is that a large fraction of cool ($<$25 000 K) white dwarfs show metals in their atmospheres. This is surprising because their high surface gravities and small (or non-existent) convection zones mean that such metals sink on short (day to Myr) time-scales implying that material is continuously accreted on to the stars with *polluted* atmospheres. It has been shown that this material does not originate from the interstellar medium (Farihi, Jura & Zuckerman 2009; Farihi et al. 2010), and its composition has been derived from atmospheric abundance patterns to be similar to terrestrial material in the Solar system (Zuckerman et al. 2007; Klein et al. 2010; Gänsicke et al. 2012). The prevailing interpretation is that asteroidal or cometary material is being accreted from a circumstellar reservoir, i.e., from the remnants of the star's debris disc and/or planetary system.

Meanwhile a complementary set of observations provides clues to the accretion process, since around 30 white dwarfs also show near-IR emission from dust (Zuckerman & Becklin 1987; Graham et al. 1990; Reach et al. 2005) and sometimes optical emission lines of metallic gas (Gänsicke et al. 2006; Farihi et al. 2012a; Melis et al. 2012) that is located within $\sim$1 $R_\odot$ from the stars. Given its close proximity to the tidal disruption radius, and the fact that all white dwarfs with evidence for hot dust or gas also show evidence for accretion in their atmospheric composition, it is thought that both the dust, gas and atmospheric pollution all arise from tidally disrupted planetesimals (Jura 2003). However, the exact nature of the disc formation process, and of the accretion mechanism are debated, which could for example be through viscous processes or radiation forces (e.g., Rafikov 2011a,b; Metzger, Rafikov & Bochkarev 2012). It is also debated whether the pollution is caused by a continuous rain of small rocks (Jura 2008), or by the stochastic accretion of much larger objects (Farihi et al. 2012b).

In this paper, we present a simple model of the accretion of planetesimals in multiple accretion events to explore how such events are manifested in observations of the star's atmospheric metal abundance. The aim is to understand how such observations can be used to derive information about the mass (or mass distribution) of accreted objects, and about whether metal-polluted atmospheres are the product of steady-state accretion of multiple objects or the accretion of single objects. A central motivation for this study is the recent claim that the distribution of inferred accretion rates is different towards stars with different principal atmospheric compositions (Girven et al. 2012; Farihi et al. 2012b), and we show how this is an important clue to determining the accretion process. While others have recently shown that the previously unmodelled stellar process of thermohaline convection can lead to substantial revision in the accretion rates inferred towards some white dwarfs, potentially removing the difference in the inferred accretion rate distributions between the two populations (Deal et al. 2013), we show here that such a difference is not unrealistic, rather it is almost unavoidable within the context of the model presented here.

In Section 2, we compile observations from the literature and use these to derive the distribution of inferred accretion rates[1] towards white dwarfs of different atmospheric properties (notably with different sinking times for metals to be removed from the atmosphere) and ages. A simple model is then presented in Section 3 that quantifies what we would expect to observe if the planetesimals being accreted on to the white dwarfs all have the same mass; Section 4 demonstrates that such a model is a poor fit to the observationally inferred accretion rate distributions, even if different stars are allowed to have different accretion rates and if the model is allowed to include a disc lifetime that moderates the way accretion is recorded on stars with short sinking times. In Section 5, the model is updated to allow stars to accrete material with a range of masses, showing that this provides a much better fit to the observationally inferred accretion rate distributions. The results are discussed in Section 6 and conclusions given in Section 7.

2 DISTRIBUTION OF ACCRETION RATES INFERRED FROM OBSERVATIONS

The accretion rate on to a white dwarf can be inferred from observations of its atmosphere, since its thin (or non-existent) convection zone means that a metal (of index i) sinks on a relatively short time-scale $t_{\rm sink(i)}$. The exact sinking time-scale depends on the metal in question and the properties of the star, but can be readily calculated (e.g., Paquette et al. 1986). In this paper, the sinking process is assumed to be gravitational settling, and so the sinking time-scale is the gravitational settling time-scale. However, to allow for the possibility that other processes act to remove metals from the convective zone (such as thermohaline convection), or indeed to replenish it (e.g., radiative levitation), we refer to sinking time-scales rather than gravitational settling time-scales throughout.

Thus, observations of photospheric absorption lines, which can be used to infer the abundance of an element at the stellar surface and by inference the total mass of that element in the convection zone $M_{\rm cv(i)}$, can be converted into an *inferred mass accretion rate* (assuming steady-state accretion, Dupuis et al. 1992, 1993a, Dupuis, Fontaine & Wosemael 1993b) of

$$\dot{M}_{\rm obs(i)} = M_{\rm cv(i)}/t_{\rm sink(i)}. \quad (1)$$

Note that $\dot{M}_{\rm obs(i)}$ is expected to differ significantly from the actual accretion rate, depending on the time variability of the accretion, as outlined in this paper; thus, we use $\dot{M}_{\rm obs(i)}$ primarily as a more convenient way of expressing $M_{\rm cv(i)}/t_{\rm sink(i)}$. Measurements of different elements provide information on the composition of the accreted material, which generally looks Earth-like (Zuckerman et al. 2007; Klein et al. 2010; Gänsicke et al. 2012), and extrapolation to any undetected metals can be used to infer a total accretion rate $\dot{M}_{\rm obs}$. It is worth emphasizing that these accretion rates are not direct observables, rather they need to be derived from stellar models (to get both $M_{\rm cv(i)}$ and $t_{\rm sink(i)}$). As such, changes in stellar models can potentially lead to significant changes in inferred accretion rates (e.g., Deal et al. 2013). The models we use in Section 2.2 are those most commonly employed in the white dwarf literature, though these have yet to incorporate the effects of thermohaline convection.

[1] Note that the rates we use here do not include the effect of thermohaline convection, the effects of which have yet to be fully characterized in this context.

Downloaded from https://academic.oup.com/mnras/article/439/4/3371/1151716 by guest on 24 March 2022

Although the literature includes many studies that measure accretion rates towards white dwarfs (e.g., fig. 8 of Girven et al. 2012), for our purposes we will require the distribution of accretion rates, i.e., the fraction of white dwarfs that exhibit accretion rates larger than a given value $f(> \dot{M}_{\rm obs})$, for which information about non-detections is as important as that about detections. Thus, here we perform a uniform analysis of data available in the literature for samples chosen to be unbiased with respect to the processes that may be causing atmospheric pollution.

From the outset, it is important to note that this paper will distinguish between two different atmospheric types: DA white dwarfs that have H-dominated atmospheres, and non-DA white dwarfs (comprised of basic sub-types DB and DC) that have He-dominated atmospheres. This distinction is necessary, because metals have very different sinking times in the two different atmospheres, and observations towards co-eval DA and non-DA white dwarfs have different sensitivities to convection zone mass. This distinction is discussed further in Section 2.1, then Section 2.2 describes the uniform analysis employed, Section 2.3 describes the unbiased DA and non-DA samples, and the distributions of accretion rates inferred from the observations are described in Section 2.4, while Section 2.5 discusses uncertainties in the inferred accretion rate distributions from the choice of model used to derive those rates.

2.1 DA versus non-DA stars

An implicit assumption adopted here is that populations of both DA and non-DA white dwarfs undergo the same history of mass input rate into the convection zone; i.e., two white dwarfs that are the same age can have different mass input rates, but the distribution of mass input rates experienced by white dwarfs of the same age is independent of their atmospheric type. There are several channels by which both DA and non-DA white dwarfs might form. However, most white dwarfs with He-dominated atmospheres (i.e., the non-DAs) are thought to form from very efficient H-shell burning in the latter stages of post-main-sequence evolution, or late thermal pulses that dilute the residual H-rich envelope with metal-rich material from the interior (e.g., Althaus et al. 2010). So, as long as these processes are not biased in terms of stellar mass, or in terms of planetary system properties, then it is reasonable to expect that the parent stars (and circumstellar environments) of DA and non-DA white dwarf populations should be similar. Indeed, observationally the mean mass of DB white dwarfs is very close to that of their DA counterparts (e.g., Bergeron et al. 2011), though a small difference has recently been discerned with DBs being slightly more massive ($0.65\,{\rm M}_{\odot}$ versus $0.60\,{\rm M}_{\odot}$; Kleinman et al. 2013). The low ratio of DB to DA white dwarfs in globular clusters (Davis et al. 2009) also suggests that the two populations could have different distributions of formation environments; our assumption requires that this difference does not significantly affect the planetary system properties (Zuckerman et al. 2010). Practically, this assumption means that we expect the observationally inferred distribution of accretion rates, $f(> \dot{M}_{\rm obs})$, to depend both on stellar age (because of evolution of the circumstellar material) and on sinking time (because that affects how the accretion rate is sampled), but not on the details of whether the star is a DA or a non-DA.

2.2 Uniform analysis

The uniform analysis consists of using reported measurements of atmospheric Ca/H (for DAs) or Ca/He (for non-DAs) for stars for which their effective temperature $T_{\rm eff}$ is also known. These abundance measurements had been derived from modelling of stellar spectra and were multiplied by the total convection zone mass (or that in the envelope above an optical depth $\tau_R = 5$; Koester 2009) to get the mass of Ca in that region. The effective temperature is used to determine the sinking time-scale of Ca due to gravitational settling, $t_{\rm sink(Ca)}$, for the appropriate atmospheric type using the models of Koester (2009), and then the convection zone mass is converted into a mass accretion rate of Ca. This rate is scaled up by assuming that the Ca represents 1/62.5 of the total mass of metals accreted, like the bulk Earth, which appears broadly supported by data for stars with Ca, Fe, Mg, Si, O and other metals detected (Zuckerman et al. 2010).

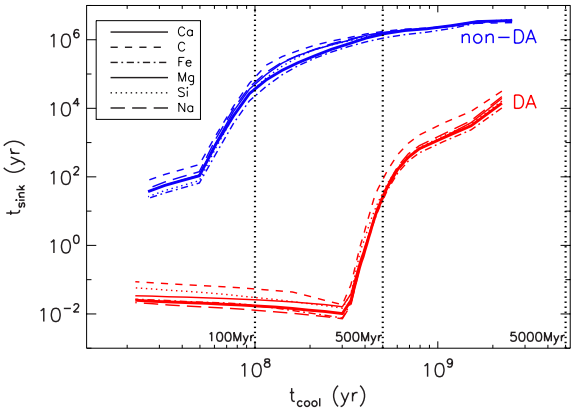


Figure 1. Sinking time-scales due to gravitational settling at the base of the convection zone (or at an optical depth of $\tau_R = 5$ if this is deeper) of different metals (shown with different line-styles as indicated in the legend) as a function of the star's cooling age (from tables 4– 6 of Koester 2009) both for DA white dwarfs (i.e., those with H-dominated atmospheres, shown in red) and for non-DA white dwarfs (i.e., those with He-dominated atmospheres, shown in blue). We adopt the parameters for more efficient mixing in DAs cooler than 13 000 K.

The other parameter of interest is the star's cooling age $t_{\rm cool}$. Although cooling age is actually a function of $T_{\rm eff}$ and $\log g$, in practice the surface gravity is poorly known due to insufficient observational data and a lack of good parallax measurements. Thus, throughout this paper we have assumed all stars to be of typical white dwarf mass[2] with $\log g = 8.0$, so that $T_{\rm eff}$ maps uniquely on to a corresponding $t_{\rm cool}$, which also then maps on to a corresponding $t_{\rm sink(i)}$. Using this assumption, Fig. 1 reproduces the sinking times due to gravitational settling of a few metals as a function of cooling age from Koester (2009) for both DAs and non-DAs.

Fig. 1 shows that sinking times vary only by a factor of a few for different metals in the same star, but that there is a large difference in sinking time-scale of a given metal when put in the atmosphere of the same star at different ages, and for stars of the same age but of different atmospheric type. For the DA white dwarfs, $t_{\rm sink}$ can be as short as a few days (e.g., Koester & Wilken 2006), whereas for the non-DA white dwarfs $t_{\rm sink}$ is more typically 0.01–1 Myr (e.g. Koester 2009). The dependence of sinking time on cooling age is similar for both atmospheric types in that it is shorter at younger ages (i.e., at high effective temperatures), followed by a transition

[2] Given the narrow distribution in white dwarf masses estimated from gravitational redshifts (Falcon et al. 2010), the uncertainty in cooling age from this assumption would be expected to be <6 per cent.

Downloaded from https://academic.oup.com/mnras/article/439/4/3371/1151716 by guest on 24 March 2022

to longer sinking times once temperatures are cool enough for a significant convection zone to develop.

2.3 DA and non-DA samples

We consider two samples, one of DAs and the other of non-DAs. The DA sample is comprised of 534 DA white dwarfs of which 38 have detections of Ca, while the remaining 496 have upper limits on the presence of Ca. These data comprise two surveys: a Keck survey that specifically searched about 100 cool DA white dwarfs for Ca absorption (Zuckerman et al. 2003), and the SPY survey which took very large telescope (VLT) ultraviolet and visual echelle spectrograph (UVES) spectra of >500 nearby white dwarfs to search for radial velocity variations from double white dwarfs (SN Ia progenitors); these data are also sensitive to atmospheric Ca (Koester et al. 2005). The more accurate data were chosen in the case of duplication. These stars are randomly chosen based on being nearby and bright, and not biased in terms of the presence or absence of metals.

The non-DA sample is a small, but uniformly sampled, set of DB stars searched for metal lines with Keck high resolution echelle spectrometer (HIRES) (see table 1 of Zuckerman et al. 2010). Stars in this sample are predominantly young, with 50–500 Myr cooling ages, but are otherwise unbiased with respect to the likelihood to detect metal lines. Although additional accretion rate measurements exist in the literature for DB stars, these would only be suitable for inclusion in this study if the sample was unbiased with regard to the presence of a disc, and if non-detections were reported with upper limits on the accretion rates.

2.4 Distribution of inferred accretion rates

The left-hand panels of Fig. 2 show the inferred accretion rate data for the two samples, plotted both against age (Fig. 2a) and against sinking time (Fig. 2c). The sense of the detection bias is evident from the lower envelope of the detections in Fig. 2(a); e.g., there are far fewer detections in the younger age bins due to the higher temperature of these stars which makes Ca lines harder to detect for a given sensitivity in equivalent width (see fig. 1 of Koester & Wilken 2006).

The right-hand panels use the information in the left-hand panels to determine the distribution of inferred accretion rates $f(>\dot{M}_{\rm obs})$ for different sub-samples as outlined in the captions. For example,

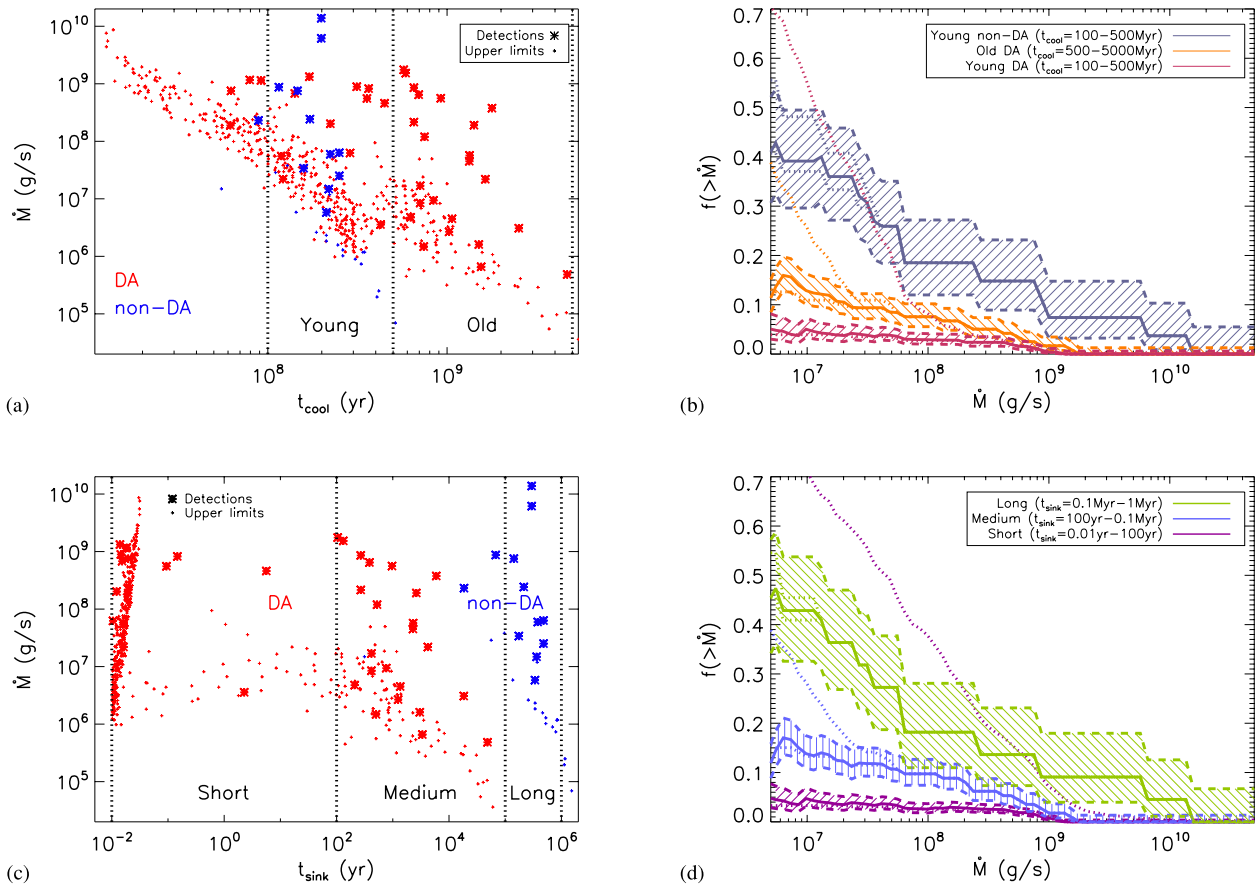


Figure 2. Inferred accretion rates for unbiased samples of DA white dwarfs (shown in red) and for non-DA white dwarfs (shown in blue). The left-hand panels (a and c) show accretion rates inferred from Ca measurements assuming a terrestrial composition. Detections are shown with asterisks and upper limits with a small plus. In (a), the x-axis is the cooling age of the white dwarf inferred from the star's effective temperature (assuming $\log g = 8.0$), whereas in (c) the x-axis is the sinking time of Ca inferred from the effective temperature. The right-hand panels (b and d) show the fraction of white dwarfs in different sub-samples that have inferred accretion rates above a given level. These sub-samples are split by cooling age in (b) into young and old age bins, and by sinking time in (d) into short, medium and long sinking time bins; the bin boundaries are noted in the legends and no distinction is made for the sub-samples in (d) between DAs and non-DAs. The dotted lines give the range of distributions inferred for each sub-sample for optimistic and pessimistic assumptions about the stars with upper limits (see the text for details). The solid lines give the best estimate of the distributions for each sub-sample, and the dashed lines and hatched regions show the 1σ uncertainty due to small number statistics (see the text for details).

Downloaded from https://academic.oup.com/mnras/article/439/4/3371/1151716 by guest on 24 March 2022

Fig. 2(b) keeps the split between DA and non-DA and further subdivides these samples according to stellar age, using age bins of 100–500 Myr (here-on the young bin) and 500–5000 Myr (here-on the old bin). Fig. 2(d) combines the DA and non-DA samples, but then makes sub-samples according to sinking time bins of 0.01–100 yr (here-on the short bin), 100 yr–0.1 Myr (here-on the medium bin) and 0.1–1 Myr (here-on the long bin), though overlap between the DA and non-DA samples is confined to a small fraction (4.4 per cent) of non-DAs in the medium bin.

Identifying the most accurate way to determine the underlying distribution of $f(> \dot{M}_{\rm obs})$ for the different sub-samples (i.e., that which would be measured with infinite sensitivity and sample size) is complicated by the fact that the observations only result in upper limits for many stars, and the sample size is finite, a problem encountered many times in astrophysics though without a definitive solution (e.g., Feigelson & Nelson 1985; Mohanty et al. 2013). Two bounds on the underlying distribution can be obtained by considering that the most pessimistic assumption for the stars that have upper limits is that they are not accreting (i.e., that with infinitely deep observations $\dot{M}_{\rm obs} = 0$), while the most optimistic assumption is that those stars are accreting at a level that is at the upper limit inferred from the observations. These bounds are plotted on Figs 2(b) and 2(d) for the different sub-samples with dotted lines, and one might expect the underlying distributions to fall between these two bounds. However, while instructive, these bounds encounter two problems. First, the optimistic limit requires the improbable occurrence of many detections at the 3σ limit. This problem is particularly acute when a significant fraction of the sample only has upper limits, such as the short sinking time sub-sample on Fig. 2(d), because not only is it statistically unlikely that the observer recorded an upper limit for each star when the true accretion level was as high as assumed in the optimistic case, but also the small number of actual detections already suggests that only a small fraction of stars should have detections at such a high level. In other words, the optimistic limit is unrealistically optimistic. The second problem is that this does not account for small number statistics, which affects in particular the distribution at high accretion rates, where the optimistic and pessimistic lines converge, but where the rates have been estimated from very few detections.

Here, we adopt an alternative method for estimating $f(> \dot{M}_{\rm obs})$ that circumvents these two problems. The idea is that if we want to know the fraction of stars in a sub-sample of size $N_{\rm s}$ that have accretion levels above say $\dot{M}_{\rm obs} = 10^7\,{\rm g\,s^{-1}}$, then we should only consider the sub-set of $N_{\rm ss}$ stars within that sub-sample for which accretion could have been detected at that level. The fraction of stars with accretion above that level is then the number of detections in that sub-set $N_{\rm ssdet}$ (noting that this may be lower than the number of stars in the whole sub-sample with accretion above that level) divided by $N_{\rm ss}$. The uncertainty on that fraction can then be determined from $N_{\rm ssdet}$ and $N_{\rm ss}$ using binomial statistics (see Gehrels 1986), and it is evident that small number statistics will be important both for large accretion rates where there are few detections (small $N_{\rm ssdet}$), and for small accretion rates where few of the sub-sample can be detected at such low levels (small $N_{\rm ss}$). In Figs 2(b) and 2(d), we show the fraction determined in this way with a solid line, and the hatched region and dashed lines indicate the 1σ uncertainty.[3]

[3] Note that these errors apply only to the measurement of $f(> \dot{M}_{\rm obs})$ at a specific accretion rate and so the points on this line are not independent of each other. This is relevant when assigning a probability that a given model provides a good fit to the data, as will be discussed later.

This method only works as long as stars are included in the sub-set in a way that does not introduce biases with respect to the level of accretion. In this case, Fig. 2(a) shows that as we try to measure the distribution down to lower levels of accretion, the only bias is that the sub-set becomes increasingly biased towards the older stars in the sub-sample. So, the distribution we infer in this way is only a good representation of that of the whole sub-sample as long as the inferred accretion rate distribution is not strongly dependent on cooling age, a topic we address below.

While Figs 2(b) and 2(d) provide the best estimate of the underlying inferred accretion rate distributions in the sub-samples, we will also use Fisher's exact test to assign a probability to the null hypothesis that two sub-samples have the same inferred accretion rate distribution. To do so, we just need four numbers, $N_{\rm ssdet}$ and $N_{\rm ss}$ for the two sub-samples measured at an appropriate accretion level, and the probability quoted will be that for the observations of these sub-samples resulting in rates that are as extreme, or more extreme, if the null hypothesis were true.

The first thing to note from Fig. 2(b) is that the distributions of inferred accretion rates in the young age bin are significantly different between the DA and non-DA populations. For example, for the sub-sets corresponding to accretion above $10^7\,{\rm g\,s^{-1}}$, there is only a 0.002 per cent probability of obtaining rates as extreme as, or more extreme than, the 4.6 per cent (6/131) of young DAs and the 39 per cent (9/23) of young non-DAs if the two are drawn from the same distribution. If as assumed in Section 2.1 the only difference between the underlying distribution of inferred accretion rates towards these stars is the sinking time-scale on which the accretion rate is measured, then this indicates that the longer sinking times of the non-DA population (with a median level of 0.37 Myr) have led to a distribution with higher inferred accretion rates than the DA population (with a median sinking time of 5 d).

Concentrating now on the inferred accretion rate distributions for the DA sub-samples in Fig. 2(b), we conclude that there is no strong evidence that these vary with age. For example, taking again sub-sets corresponding to accretion above $10^7\,{\rm g\,s^{-1}}$, there is a 2.6 per cent probability of obtaining rates as extreme as, or more extreme than, the 4.6 per cent (6/131) of young DAs and the 12.4 per cent (13/105) of old DAs if the two are drawn from the same distribution. While the small difference in rates between the populations could be indicative of an age dependence in the inferred accretion rate (higher rates around older stars), this is of low statistical significance. Moreover, since age is correlated with sinking time in the DA sub-samples (Fig. 1), and the previous paragraph concluded that longer sinking times lead to higher inferred accretion rates, it is possible that the (marginally) higher accretion rates around the older DA sub-sample are due to their longer sinking times relative to the younger DA sub-sample, and have nothing to do with the evolution of the underlying accretion rate distribution. However, it is not possible to conclude that age is not an important factor in determining the inferred accretion rate distribution, as there could even be a strong decrease in accretion rate with age that has been counteracted in the sub-samples of Fig. 2(b) by the sinking time dependence. To assess the effect of age properly would require comparison of sub-samples of DAs and non-DAs with the same sinking times but different ages, but this is not available to us for now (see Fig. 2c). Nevertheless, since we do not see any evidence for a dependence on age (see also Koester 2011), our analysis in this paper will assume the underlying distribution of accretion rates to be independent of age (noting that an age dependence in the distribution of inferred accretion rates may arise through the sinking time).

Downloaded from https://academic.oup.com/mnras/article/439/4/3371/1151716 by guest on 24 March 2022

Given that sinking time is likely the dominant factor, the most important plot is Fig. 2(d). The picture that emerges reinforces the previous conclusion on the importance of sinking time in the inferred accretion rate distributions, and furthermore points to a monotonic change in the distribution of inferred accretion rates, with longer sinking times resulting in higher inferred accretion rates. To quantify the significance of the difference between the sub-samples, take again sub-sets corresponding to accretion above 10^7 g s^{-1}; there is a 0.0006 per cent probability of obtaining levels as extreme as, or more extreme than, the 43 per cent (9/21) rate in the long bin and the 4.3 per cent (6/140) rate in the short bin if the two are drawn from the same distribution. This probability becomes 0.4 per cent when comparing the rate in the long bin with the 13.4 per cent (13/97) rate in the medium sinking time bin, and 1.1 per cent when comparing the rates in the short and medium sinking time bins (this latter probability is further reduced to ∼0.6 per cent if larger accretion rates up to 10^8 g s^{-1} are considered). That is, as expected from above, there is a significant difference between the sinking time bins, though the confidence level that all three sinking time bins have distributions that are different from each other, and hence that there is a monotonic change in inferred accretion rates across a wide range of sinking times, is slightly below 3σ.

While the above analysis is not sufficient to make a strong statement about the difference between (say) the short and medium sinking time bins, we take the near 3σ significance to indicate that future observations will soon be able to find such a difference, if it exists. Thus, we tailor the models in the following sections to reproduce as good a fit to the solid lines in Fig. 2(d) as possible. This approach allows us demonstrate the qualitative behaviour of the models, and how the different parameters affect their predictions for the dependence of the inferred accretion rate distribution on sinking time. However, in doing so we recognize that this approach may appear to constrain the model in ways that will not be formally significant given the limitations of small number statistics, and note in future sections where that is the case.

Note that while we have assumed that there is no dependence of accretion rate on age, the lack of evolution is not well constrained, and the different sinking time bins have different age distributions; the median ages are 140, 840 and 220 Myr for the short, medium and long bins, respectively. If there was a dependence of accretion rate on age, the most significant effect would likely be on the position of the medium sinking time bin with respect to the other bins. For example, a decrease in accretion rates with age would mean the distribution $f(> \dot{M}_{\rm obs})$ for the medium bin would be higher if plotted at a comparable age to that of the long and short bins.

2.5 Caveats

The method described above to derive accretion rates makes some simplifications about the evolution of accreted metals. Specifically the assumption is that metals are removed from the observable outer atmosphere over a sinking time, where the sinking time is that due to gravitational settling. This is the standard approach in the literature (e.g., Koester 2009). However, one important process that is omitted here is thermohaline (or fingering) convection. Thermohaline convection is triggered by a gradient in metallicity in the stellar atmosphere that decreases towards the centre, such as would be expected if high-metallicity material had been accreted at the surface. In such a situation, the metals can be rapidly mixed into the interior through metallic fingers, analogous to salt fingers studied in the context of Earth's oceans (e.g., Kunze 2003). Application of this process to general astrophysical situations, such as mixing in stellar atmospheres, has been characterized using 3D numerical simulations (Traxler, Garaud & Stellmach 2011; Brown, Garaud & Stellmach 2013). Thermohaline convection has been shown to have important consequences for mixing of planetary material accreted by main-sequence stars (Vauclair 2004; Garaud 2011), for stars that accreted material from an asymptotic giant branch (AGB) companion (Stancliffe & Glebeek 2008), and possibly for low-mass red giant branch stars (Denissenkov 2010).

A recent study also found that this process may be important for accretion on to white dwarf atmospheres (Deal et al. 2013), in that accretion rates inferred from observations of DA white dwarfs may actually be higher than previously considered. The rates for non-DA white dwarfs would be unaffected by this process leading to the interesting possibility that the distribution of rates for both populations are the same. However, for now the model has only been applied to six stars, and the implications have yet to be characterized across the range of stellar and pollution parameters required in this study. As such it is premature (and not possible with published information) to use rates that account for thermohaline convection in this paper. Nevertheless, since this process has the potential to affect inferred accretion rates, and may also do so in a way that depends on sinking time, a caveat is required when interpreting the conclusions in Section 2.4 about how accretion rate distributions depend on sinking time. If the rates need to be modified as a result of this process, the analysis in this paper could be repeated, and we note below the potential implications if the rate was to turn out to be independent of sinking time.

3 SIMPLE MODEL: STOCHASTIC ACCRETION OF MONO-MASS PLANETESIMALS

The dependence of inferred accretion rates on sinking time has previously been noted by Girven et al. (2012) and discussed further in Farihi et al. (2012b) from a difference between the accretion rates inferred towards DA and non-DA populations. It is interpreted as evidence of the stochastic nature of the accretion process, with the short sinking time DAs providing a measure of the *instantaneous* level of accretion being experienced by the star, and the longer sinking time of non-DAs providing evidence for *historical* accretion events, such as the accretion of a large comet which can leave mass in the atmospheres of non-DAs for long periods after the event. In this section, we use a pedagogical model to illustrate the nature of stochastic processes and to quantify how different mass accretion rates (of objects of finite mass) would be expected to be inferred towards white dwarf populations with different sinking times.

3.1 Pedagogical model

Consider a white dwarf at which planetesimals are being thrown at a mean rate $\dot{M}_{\rm in}$. Here, it is assumed that all planetesimals have the same mass $m_{\rm p}$, and that once accreted at time t_i, the mass from planetesimal i that remains potentially visible in observations of the white dwarf's atmosphere decays exponentially on the sinking time $t_{\rm sink}$, i.e., for $t > t_i$

$$m_{{\rm atm},i} = m_{\rm p} {\rm e}^{(t_i - t)/t_{\rm sink}}. \quad (2)$$

Note that after being accreted, the planetesimal is mixed nearly instantaneously within the white dwarf's convective zone, and only a small fraction of that mass contributes to the observable atmospheric signatures at any one time. Thus, by $m_{{\rm atm},i}$ we really mean the mass of planetesimal i that remains in the convective zone, which can be determined through observations of abundances in the white dwarf's

Downloaded from https://academic.oup.com/mnras/article/439/4/3371/1151716 by guest on 24 March 2022

atmosphere using a stellar model to determine the total mass of the convective zone over which that abundance is assumed to apply.

The total mass of pollutants that are present in the convective zone, and hence potentially visible in the white dwarf's atmosphere at any one time, which we call the atmospheric mass, is the sum of all previous accretion events, depleted appropriately by the decay, i.e.,

$$M_{\rm atm} = \sum_i m_{{\rm atm},i}. \tag{3}$$

We also define the accretion rate that would be inferred from such an atmospheric mass as

$$\dot{M}_{\rm atm} = M_{\rm atm}/t_{\rm sink}. \tag{4}$$

Note the similarity with equation (1), which is because we will be comparing $\dot{M}_{\rm atm}$ with $\dot{M}_{\rm obs}$, and underscores the importance of using the same value of $t_{\rm sink}$ in the modelling as that used to obtain accretion rates from the observations.

Since the mass can only arrive in units of $m_{\rm p}$, this is a Poisson process, and $\dot{M}_{\rm atm}$ is not necessarily equal to $\dot{M}_{\rm in}$. Rather the inferred accretion rate has a probability density function $P(\dot{M}_{\rm atm})$, and an associated cumulative distribution function that we characterize by

$$f(>\dot{M}_{\rm atm}) = \int_{\dot{M}_{\rm atm}}^{\infty} P(x)\,{\rm d}x, \tag{5}$$

which is the fraction of the time we would expect to measure an accretion rate larger than a given value.

The set-up of this problem is exactly the same as that for shot noise, the nature of which depends on the parameter n, the mean number of shots per unit time (see Appendix A). For our problem,

$$n = \dot{M}_{\rm in} t_{\rm sink}/m_{\rm p} \tag{6}$$

is the mean number of accretion events per sinking time, and the shots have the form

$$F(\tau) = H(\tau){\rm e}^{-\tau}, \tag{7}$$

where $\tau = t/t_{\rm sink}$ is time measured in units of the sinking timescale, $H(\tau)$ is the Heaviside step function, and the *shot amplitude* discussed in the appendix and references therein should be scaled by $m_{\rm p}/t_{\rm sink}$ to get this in terms of the inferred accretion rate.

Here, we derive the cumulative distribution function using a Monte Carlo model (Section 3.2), and apply results from the literature for shot noise to explain the shape of the distribution function analytically (Section 3.3).

3.2 Monte Carlo model

For a white dwarf with a given $t_{\rm sink}$, and accretion defined by $\dot{M}_{\rm in}$ and $m_{\rm p}$, we first define a timestep ${\rm d}t = t_{\rm sink}/N_{\rm sink}$, where $N_{\rm sink}$ is the number of timesteps per sinking time (this should be large enough to recover the shape of the exponential decay of atmospheric mass, and is set to 10 here). We then set a total number of timesteps, $N_{\rm tot}$ (set to 200 000 here), and use Poisson statistics to assign randomly the number of planetesimals accreted in each timestep (using the *poidev* routine, Press et al. 2007, and a mean of $\dot{M}_{\rm in}{\rm d}t/m_{\rm p}$). The $N_{\rm tot}$ timesteps are considered as a (looped) time series, and so the mass accreted in each timestep is carried forward to subsequent timesteps with the appropriate decay (equation 2) to determine the mass in the atmosphere and inferred accretion rate as a function of time.

Fig. 3 shows the result of this process for canonical parameters of $\dot{M}_{\rm in} = 10^{10}\,{\rm g\,s^{-1}}$ and $m_{\rm p} = 3.2 \times 10^{19}$ g. This accretion rate corresponds to the mass of the current asteroid belt (Krasinsky et al.

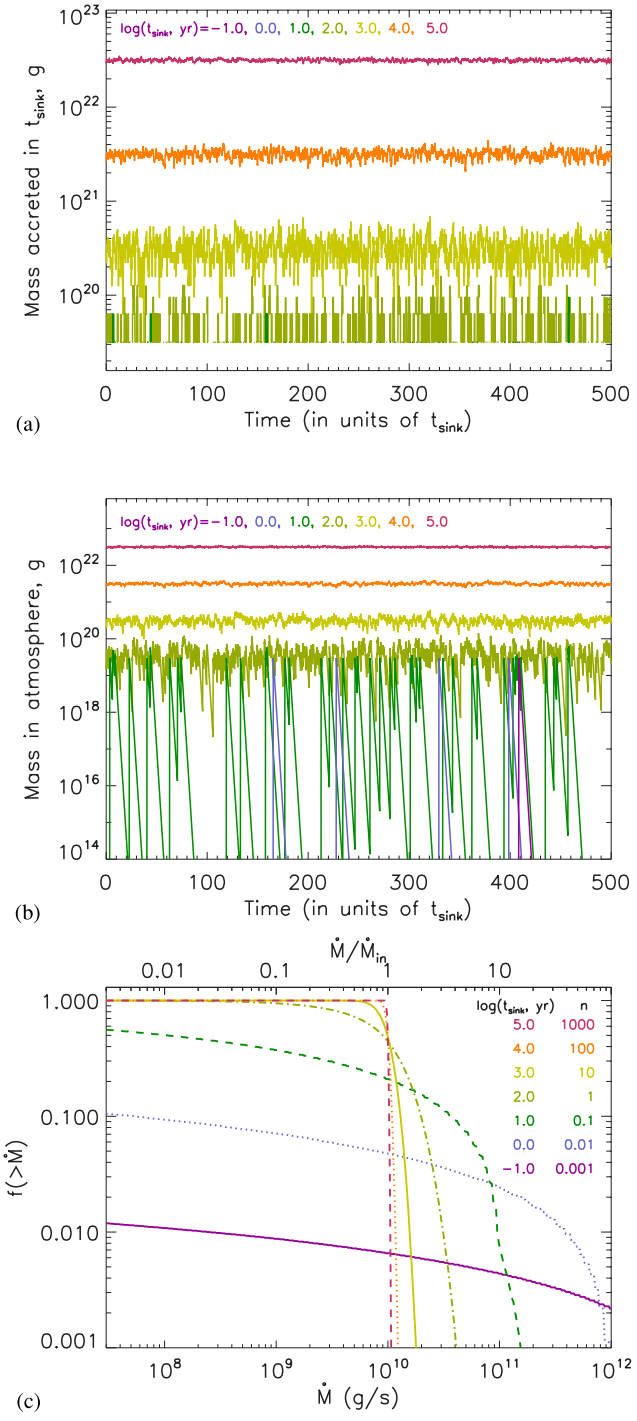


Figure 3. Monte Carlo simulations of accretion of 3.2×10^{19} g planetesimals at a mean rate $10^{10}\,{\rm g\,s^{-1}}$ on to white dwarfs with seven different sinking times $t_{\rm sink}$ logarithmically spaced between 0.1 yr and 0.1 Myr shown with different colours. (a) The total mass accreted in one sinking time, as a function of time, with only the first 500 sinking times shown for clarity. (b) The total mass remaining as potentially visible in the atmosphere as a function of time. (c) The fraction of all timesteps for which the accretion rate is measured to be above the rate given on the x-axis; i.e., the cumulative distribution function $f(>\dot{M}_{\rm atm})$. The top axis generalizes this plot to dimensionless accretion rate ($\dot{M}/\dot{M}_{\rm in}$) when used in conjunction with the number of accretion events per sinking time (n) given in the legend.

Downloaded from https://academic.oup.com/mnras/article/439/4/3371/1151716 by guest on 24 March 2022

2002) being accreted every ∼10 Myr. This planetesimal mass corresponds to a 27 km diameter planetesimal for a density of 3 g cm^{-3}, and has been chosen so that a sinking time of 100 yr corresponds to a mean rate of one planetesimal being accreted per sinking time (i.e., $n = 1$). This process has been repeated for seven different sinking times that correspond to $n = 0.001$, 0.01, 0.1, 1, 10, 100 and 1000 planetesimals being accreted per sinking time.

Fig. 3(a) shows how longer sinking times (larger n) result in larger quantities of mass accreted in one sinking time. However, decreasing the sinking time runs into a barrier since the accreted mass cannot be less than the mass of a single planetesimal. Thus, as n is decreased to 1 and below, the mass accreted in any one sinking time becomes more noticeably probabilistic. The same effect is also seen in Fig. 3(b), except that the mass remaining as potentially visible in the atmosphere can be less than m_p. Indeed for the shortest sinking times of 0.1 and 1 yr, the atmospheric mass spends most of its time at insignificantly small levels, increasing to the level of m_p only immediately following an accretion event, with exponential decay thereafter. In contrast, for the longest sinking times ($n \gg 1$), the atmospheric mass is approximately constant at a level $\dot{M}_{in} t_{sink}$.

The distribution of atmospheric masses is quantified in Fig. 3(c), which shows the fraction of time the accretion rate would be inferred to be above a given level. For long sinking time-scales ($n \gg 1$), this is close to a step function, transitioning from 1 to 0 close to $\dot{M}_{in}$; i.e., the inferred accretion rate is always very close to the mean level. For short sinking time-scales ($n \ll 1$), however, the inferred accretion rate covers a broad range, from around m_p/t_{sink} just after an accretion event, which is significantly higher than $\dot{M}_{in}$ in this regime, down to levels far below $\dot{M}_{in}$. As noted in Section 3.3, the distribution at levels just below m_p/t_{sink} in this regime is to a reasonable approximation dictated by the exponential decay function, since intermediate accretion rates are simply the vestiges of earlier accretion events.

3.3 Analytical

The distribution of shot noise characterized in the manner of equations (6) and (7) is given in section 6.1 of Gilbert & Pollack (1960) (see Appendix A). There they derive the exact form of the probability density distribution for $\dot{M}_{atm} < m_p/t_{sink}$ (or equivalently for $\dot{M}_{atm}/\dot{M}_{in} < n^{-1}$) as

$$P(\dot{M}_{atm}) = \left(\frac{t_{sink}}{m_p}\right)^n \frac{e^{-n\gamma}}{\Gamma(n)} \dot{M}_{atm}^{n-1}, \quad (8)$$

where $\gamma \approx 0.577\,215\,665$ is Euler's constant and $\Gamma(n)$ is the gamma function (see equation A6). This means that the cumulative density distribution is

$$f(> \dot{M}_{atm}) = 1 - \frac{e^{-n\gamma}}{n\Gamma(n)} \left(\frac{\dot{M}_{atm} t_{sink}}{m_p}\right)^n. \quad (9)$$

Rather than compare this prediction directly with the distribution derived from the Monte Carlo model in Fig. 3(c), we instead use those distributions to find the 1 per cent, 10 per cent, 50 per cent and 90 per cent points in the distribution, repeat for a larger number of sinking times, and plot these as a function of t_{sink} in Fig. 4. Abbreviating $f(> \dot{M}_{atm})$ to f for now, the prediction is that

$$\dot{M}_{atm}(f) = \left(\frac{m_p}{t_{sink}}\right) [(1-f) n \Gamma(n) e^{n\gamma}]^{1/n}, \quad (10)$$

which will be valid as long as the quantity in square brackets is less than 1 (e.g., for $n = 1$, i.e. $t_{sink} = 100$ yr, this is valid for $f > 1 - e^{-\gamma} \approx 0.44$). This is plotted in purple on Fig. 4 showing excellent agreement with the Monte Carlo model, noting that deviations from the analytical prediction are expected due to small number statistics.

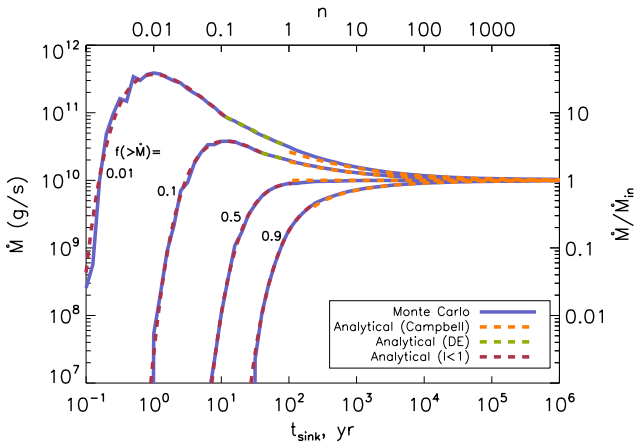


Figure 4. Simulations of accretion of 3.2×10^{19} g planetesimals at a mean rate 10^{10} g s^{-1} on to a white dwarf with a sinking time t_{sink}. The lines show the distribution of inferred accretion rates; e.g., the top line corresponds to the level that would be exceeded in 1 per cent of measurements, while the $f(> \dot{M}_{atm}) = 0.5$ line is the median of the distribution. The blue solid line shows the results of an expanded set of Monte Carlo simulations similar to those shown in Fig. 3. The dashed lines show various analytical estimates discussed in the text: the $\dot{M}_{atm} < m_p/t_{sink}$ solution in purple, the solution to the Gilbert & Pollack (1960) differential difference equation in green, and Campbell's theorem in orange. The top and right axes generalize this plot to dimensionless accretion rate ($\dot{M}/\dot{M}_{in}$) as a function of number of accretion events per sinking time (n).

For heuristic purposes, it is also worth pointing out that the distributions in the limit of $n \ll 1$ for $f(> \dot{M}_{atm}) \ll 1$ are asymptotically the same as would be expected had we imagined planetesimals to arrive at regularly spaced intervals of t_{sink}/n in time. In that case, the fraction of time we would expect to infer accretion rates of different levels would be determined by the exponential decay, and so

$$f(> \dot{M}_{atm}) = n \ln\left[\frac{m_p}{\dot{M}_{atm} t_{sink}}\right] \quad (11)$$

in the range 1 to $e^{-1/n}$ times m_p/t_{sink}.

There is no exact solution for the distribution at higher accretion rates ($\dot{M}_{atm} > m_p/t_{sink}$), however Gilbert and Pollack provide a differential difference equation that can be solved to determine $P(\dot{M}_{atm})$ (see equation A5). We show the resulting solution in green on Fig. 4, but only over a limited region of parameter space as validation of the technique, and of the Monte Carlo model, since these are essentially different numerical methods of obtaining the same answer.

However, there is an asymptotic solution in the large n regime (i.e., large t_{sink}). Campbell's theorem (Campbell 1909a,b) can be applied to show that the probability density function in this limit becomes a Gaussian with a mean of $\dot{M}_{in}$ (see equations A8 and A9)

$$P(\dot{M}_{atm}) = \left(\frac{t_{sink}}{m_p}\right) \frac{1}{\sqrt{2\pi\sigma^2}} e^{-\frac{1}{2\sigma^2}(\dot{M}_{atm} - \dot{M}_{in})^2}, \quad (12)$$

where the variance $\sigma^2 = n(m_p/t_{sink})^2/2$. This means that the cumulative distribution function is

$$f(> \dot{M}_{atm}) = [1 - \mathrm{erf}(x)]/2, \quad (13)$$

Downloaded from https://academic.oup.com/mnras/article/439/4/3371/1151716 by guest on 24 March 2022

where erf(x) is the error function of $x = \frac{\dot{M}_{\rm atm} - \dot{M}_{\rm in}}{\sqrt{\dot{M}_{\rm in} m_{\rm p}/t_{\rm sink}}}$. Equation (13) can be solved to get the appropriate points in the distribution shown in orange in Fig. 4 for $n > 1$. This shows that Campbell's theorem provides an adequate approximation for large n, but that discrepancies become noticeable as n approaches 1.

4 CAN A MONO-MASS PLANETESIMAL DISTRIBUTION FIT THE OBSERVATIONS?

It is clear from Section 3 that even with a very simple model, in which planetesimals have the same mass around all stars, and in which all stars are accreting matter at the same mean rate, it is expected that a broad distribution of accretion rates could be inferred observationally, and that this distribution could be different towards white dwarfs with different sinking times. However, in Section 4.1 we explain why such a simple model cannot explain the observationally inferred rates of Section 2. Then in Section 4.2, we explore the possibility that all stars have planetesimals that are the same mass, but that different stars have different mean accretion rates, again ruling this out. In Section 4.3, we consider how these conclusions may be affected if planetesimals are processed through a disc on a time-scale that can exceed the sinking time-scale before being accreted.

Throughout the paper, we quantify the goodness of fit for a model in a given sinking time bin s as

$$\chi_s^2 = \sum_j \left(\frac{f(> \dot{M}_{{\rm obs}(j,s)}) - f(> \dot{M}_{{\rm atm}(j,s)})}{\sigma[f(> \dot{M}_{{\rm obs}(j,s)})]} \right)^2, \qquad (14)$$

where $f(> \dot{M}_{{\rm obs}(j,s)})$ is the best estimate from the observations of the fraction of stars in bin s with accretion above a level denoted by the index j, where the sum is performed for j corresponding to $10^7, 10^8, 10^9$ and 10^{10} g s^{-1}, $\sigma[f(> \dot{M}_{{\rm obs}(j,s)})]$ is the larger of the positive or negative 1σ uncertainties plotted in Fig. 2(d), and $f(> \dot{M}_{{\rm atm}(j,s)})$ is the corresponding model distribution. Since the observables in a cumulative distribution (i.e., $f(> \dot{M}_{{\rm obs}(j,s)})$) are not independent at the different indices, the absolute value of χ_s^2 should not be used to determine the formal significance of the model fit to the data. Rather we will be using it here as a relative measure of the goodness of fit of different models for a given bin.

4.1 Mono-mass, mono-rate accretion

The distribution of inferred accretion rates for a mono-mass mono-rate model will always have a dependence on sinking time that is similar in form to that shown in Fig. 3(c). Varying the mean accretion rate parameter, $\dot{M}_{\rm in}$, would simply change the x-axis scaling such that the distributions for the longest sinking times all have accretion rates inferred at the $\dot{M}_{\rm in}$ level (see top axis). Varying the planetesimal mass would change the sinking times corresponding to the different lines on the figure, but these lines would always correspond to the same n given in the legend (e.g., the green line corresponds to $n = 1$), and so equation (6) can be used to work out the corresponding sinking time which just scales with planetesimal mass (e.g., the pale green line corresponds to $t_{\rm sink} = m_{\rm p}/\dot{M}_{\rm in}$).

Fig. 2(d) provides several clues as to what combination of $\dot{M}_{\rm in}$ and $m_{\rm p}$ would be required to reproduce any given distribution. For example, the fact that the $\dot{M}_{\rm obs}$ distribution is broad for all of the sinking time bins means that $n \ll 1$ for all of the bins. The breadth of the distribution is indicative of the n required to fit any of the relevant lines, and the appropriate value for the long sinking time-scale bin

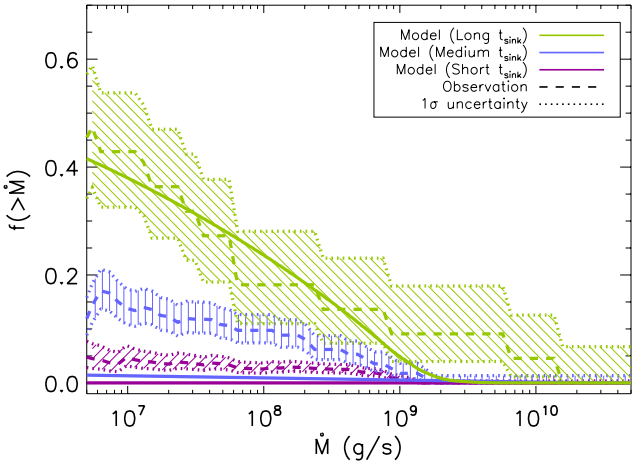


Figure 5. Simulations of accretion of 2.2×10^{22} g planetesimals at a mean rate 1.7×10^8 g s^{-1} on to populations of white dwarfs with distributions of sinking times that match that of the corresponding observed populations in each of the sinking time bins. The dashed lines show the distribution inferred from the observations, while the hatched regions and dotted lines show the $\pm 1\sigma$ range of possible distributions given small number statistics (reproduced from Fig. 2d). The model predictions are shown with solid lines in the corresponding colour. The model for the short sinking time bin is indistinguishable from 0 on this plot.

can be inferred readily from Fig. 4 using the top and right axes. That is, for there to be a range of around 1000 in accretion rates between the 10 per cent and 50 per cent points in the distribution requires $n \approx 0.09$. The input accretion rate can then be found by scaling the 50 per cent point to be close to 10^6 g s^{-1} (Fig. 2d) giving an $\dot{M}_{\rm in}$ of around 1.7×10^8 g s^{-1}, and so a planetesimal mass $m_{\rm p}$ of around 2.2×10^{22} g (for the median sinking time of 0.37 Myr in this bin).

Fig. 5 reproduces the inferred accretion rate distributions of Fig. 2(d) and also makes predictions for model populations in which stars have the same distributions of sinking times as that of the observed population in the corresponding bin, under the assumption that all stars are accreting 2.2×10^{22} g planetesimals (i.e., roughly 240 km diameter asteroids) at a mean rate 1.7×10^8 g s^{-1} (equivalent to around one asteroid belt every 680 Myr). This model population was implemented by taking each star in the corresponding observed population and running the Monte Carlo model of Section 3.2 with the sinking time for that star, then combining the results for all stars into one single population. The number of timesteps used for each star, $N_{\rm tot}$, was chosen so that the total number of accretion rates used for the model population (i.e., $N_{\rm tot}$ times the number of stars in the observed population) was close to 10^5.

As expected from the arguments two paragraphs ago, a model with these parameters gives a decent fit to the long sinking time bin (for reference $\chi_s^2 = 1.0$ as defined in equation 14). However, the same model provides a very poor fit to the shorter sinking time bins ($\chi_s^2 = 12$ and 21 in the short and medium sinking time bins, respectively). The problem is that having $n \ll 1$ in the long bin means that such time-scales are already sampling the vestiges of past events (i.e., such events happen much less frequently than once per Myr). This means that, while it is possible for measurements with shorter sinking times to infer high accretion rates just after the event, such measurements would be extremely rare. By consequence, we would expect to see essentially no accretion signatures in the samples with $t_{\rm sink} < 0.1$ Myr (see Fig. 5).

Downloaded from https://academic.oup.com/mnras/article/439/4/3371/1151716 by guest on 24 March 2022

4.2 Mono-mass, multirate accretion

One conclusion from Section 4.1 is that, for a mono-mass distribution of planetesimal masses, a model that fits all sinking time bins simultaneously requires $n \gg 1$ for (the majority of) the long sinking time bin. The broad distribution of observationally inferred accretion rates in this bin, $f(> \dot{M}_{\rm obs})$, thus implies that different stars accrete at different rates, and that the observationally inferred distribution is representative of that of the mean rate at which material is being accreted, $f(> \dot{M}_{\rm in})$. At least this must be the case for high accretion rates, but it is possible that the lowest accretion rates, say below $\dot{M}_{\rm in} = 10^7\,{\rm g\,s^{-1}}$, are in the $n < 1$ regime. This also sets a constraint on the planetesimal mass, since requiring $n > 1$ in the $\sim$0.37 Myr sinking time bin for $\sim 10^7\,{\rm g\,s^{-1}}$ means that $m_{\rm p} < 10^{20}$ g.

Here, we modify the population model of Section 4.1 by assuming that different white dwarfs accrete at different rates, i.e. that there is a distribution $f(> \dot{M}_{\rm in})$, but from the same mono-mass distribution of planetesimal masses, $m_{\rm p}$. Practically this is implemented in the model population by each of the observed stars in the appropriate sample having its accretion rate chosen randomly from the given distribution a sufficient number of times to get a total of $\sim$1000 combinations of $t_{\rm sink}$ and $\dot{M}_{\rm in}$, which are then simulated at 1000 timesteps. For an assumed planetesimal mass, we proceed by using the long sinking time bin to constrain the distribution $f(> \dot{M}_{\rm in})$. Comparison of the model predictions to the observationally inferred rates for all sinking time bins is then used to determine the planetesimal mass that gives the best overall fit.

The simplest form for the distribution of $\dot{M}_{\rm in}$ is log normal, with a median of $10^{\mu}\,{\rm g\,s^{-1}}$ and width of σ dex. As pointed out above, if the planetesimal mass is small enough this distribution should be defined by the distribution of rates inferred in the long sinking time bin. By minimizing χ^2_s for the long bin, the median and the width of the observationally inferred distribution were found to be $\mu = 6.6$ and $\sigma = 1.5$, and we confirmed that using this for the input accretion rate, $f(> \dot{M}_{\rm in})$, gives a reasonable fit to the long sinking time bin provided that $m_{\rm p} < 10^{20}$ g.

As $m_{\rm p}$ is increased above 10^{20} g, the input accretion rate distribution given in the last paragraph no longer provides a reasonable fit to the long sinking time bin, as a larger fraction of stars in the sample have $n < 1$. To get around this, the input accretion rate needs to be higher (because the inferred rate is lower for most stars when $n < 1$) and the width of the distribution narrower (since decreasing n leads to a broader distribution of inferred accretion rates). The parameters of a log-normal input accretion rate distribution that give the minimum χ^2_s for the long sinking time bin are given in Fig. 6(a) as a function of assumed planetesimal mass. As can be seen, these tend to the values given in the last paragraph for small $m_{\rm p}$, and change in the sense expected as $m_{\rm p}$ is increased.

Fig. 6(b) shows how the resulting goodness of fit χ^2_s varies for all sinking time bins as $m_{\rm p}$ is changed. This shows that it is not possible to maintain a reasonable quality fit to the long bin with high $m_{\rm p}$. This is inevitable, because in the regime of large $m_{\rm p}$ (i.e., small n), the distribution of inferred accretion rates necessarily becomes very broad even for input distributions that are very narrow (see Figs 3c and 4), and eventually become much broader than that inferred from the observations. Thus, the best fit will tend to one in which the model has too many high accretion rates, but too few low accretion rates. It is no coincidence that the best fit to this bin starts to get significantly worse beyond around $m_{\rm p} = 2 \times 10^{22}$ g at a point close to $\mu = 8.2$ and $\sigma = 0$, which was the best fit of Section 4.1.

Even for planetesimal masses where a reasonable fit to the long sinking time bin is possible, it is not possible to simultaneously find an acceptable fit to both shorter sinking time bins. Fig. 6(b) shows how χ^2_s varies with planetesimal mass, and Fig. 6(c) shows the best fit that minimizes the sum of χ^2_s for all bins, which is for $m_{\rm p} = 1.0 \times 10^{20}$ g. For example, consider the medium sinking

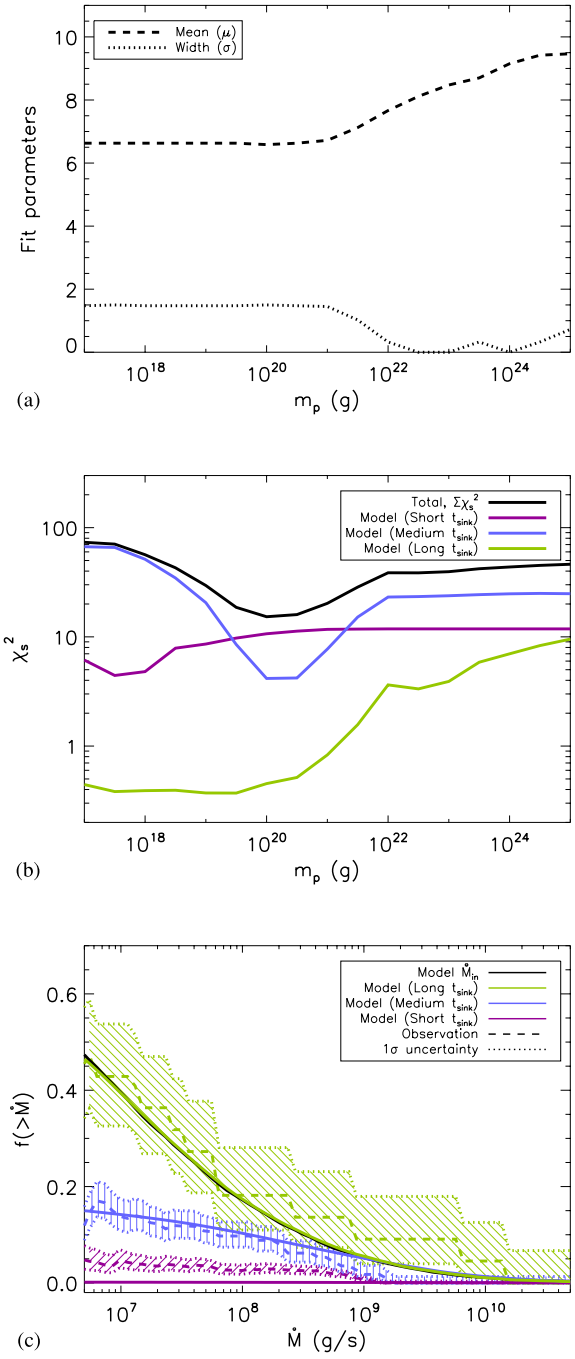


Figure 6. Simulations of accretion of planetesimals all of mass $m_{\rm p}$, at a mean rate drawn from a log-normal distribution described by the parameters μ and σ for populations with the same distribution of sinking times as the stars observed in the corresponding bins in Fig. 2(d). (a) Parameters for the input accretion rate distribution that give a best fit to the long sinking time bin. (b) The goodness of fit χ^2_s to the three different bins as a function of $m_{\rm p}$. (c) Comparison of the model populations to the rates inferred from the observations for the parameters providing the best (but still not great) fit to all bins, which is for $m_{\rm p} = 1.0 \times 10^{20}$ g (see (b)). The model for the short sinking time bin is indistinguishable from 0 on this plot.

Downloaded from https://academic.oup.com/mnras/article/439/4/3371/1151716 by guest on 24 March 2022

time bin. For the smallest planetesimal masses, $n \gg 1$ for all stars in this bin and so the distribution of inferred rates for the model population is close to that for the input rates; i.e., the model population has too many large accretion rates. Increasing planetesimal mass decreases n for all stars, and a crude approximation is that the resulting distribution remains close to that of the input rates for large accretion rates, but becomes flat at accretion rates for which $n \ll 1$ for the bin's median sinking time of 850 yr, corresponding to $\dot{M} \ll 3.7 \times 10^9$ g s^{-1} on Fig. 6(c) (compare the black and blue lines); a similar analysis for the long sinking time bin explains why the model's inferred accretion rate distribution (the green line on Fig. 6c) only departs from the input rate distribution (black line) below 9×10^6 g s^{-1}. Increasing planetesimal mass above the best fit of 1.0×10^{20} g results in the model population having a negligible fraction with accretion rates in the appropriate range. The situation is similar for the short sinking time bin (see Fig. 6b), except that the model population is closest to that inferred from the observations (albeit slightly flat) when the planetesimal mass is just below 10^{18} g, with essentially no accretion signatures expected in this bin by the time the planetesimal mass is large enough to fit the medium bin (Fig. 6c).

In conclusion, although the best fit has improved relative to Section 4.1, it is not possible to provide a reasonable fit to the distribution of accretion rates inferred from the observations within the constraints of this model. In Section 4.3, we explore whether this is primarily an (avoidable) consequence of having so many orders of magnitude difference in sinking times between the bins.

4.3 Finite disc lifetime

The assumption thus far is that the entire planetesimal mass is placed in the stellar atmosphere on a time-scale that is much shorter than the sinking time-scale. If material were accreted by direct impact on to the star this would be reasonable. However, accretion by direct impact is considered unlikely since the stellar radius is so much smaller (∼70 times) than the tidal disruption radius, meaning that material is likely to tidally disrupt and form a disc before whatever process that kicked it to 1 R$_\odot$ gets it on to the star (Farihi et al. 2012b). Indeed observations support the notion that material is processed through a disc that is sometimes detectable (see Section 1). The lifetime of such discs and the physical mechanisms by which material is accreted on to the star are active topics of discussion (Rafikov 2011a,b; Farihi et al. 2012b; Metzger et al. 2012). Various time-scales are involved, such as that to circularize the orbits of tidally disrupted planetesimals, that to convert this material into dust, that to make the dust reach the sublimation radius where it is converted into gas and that for gas to accrete on to the star. Nevertheless, it would not be unreasonable to assume that this process takes many years, since the viscous time for gas to get from the sublimation radius to the star is at least 100–1000 yr (Farihi et al. 2012b; Metzger et al. 2012).

To model the disc properly requires significant modifications to the model that are beyond the scope of this paper. Instead the disc will be considered here with the simplest prescription that is readily implemented into the model. Thus, we assume that all discs have the same lifetime $t_{\rm disc}$, and that following accretion (by which we really mean incorporation into the disc), the planetesimal mass present in the atmosphere decays on a time-scale

$$t_{\rm samp} = \sqrt{t_{\rm disc}^2 + t_{\rm sink}^2}. \quad (15)$$

Effectively this means that, even if a star has a sinking time of a few days, the time-scale over which observations of the atmospheric pollution are sampling the accretion rate can be longer, and this time-scale is roughly equal to the larger of the disc lifetime and the sinking time. The question then is whether this additional parameter is sufficient to allow us to fit the distributions inferred from the observations, and if so what is the typical disc lifetime.

4.3.1 *Mono-mass, mono-rate with disc lifetime*

In Fig. 7, we repeat the modelling of Section 4.1 to show that a reasonable fit could be obtained simultaneously with both the long bin and either the medium bin (with $t_{\rm disc} \approx 0.084$ Myr) or the short bin (with $t_{\rm disc} \approx 0.013$ Myr), but that it is not possible to fit all bins simultaneously. The problem is that disc lifetimes of >0.01 Myr are so high that the sampling times for the populations of both shorter time-scale bins are set by the disc lifetime and so are very similar. Consequently, their inferred accretion rate distributions are indistinguishable. For these bins to have different distributions

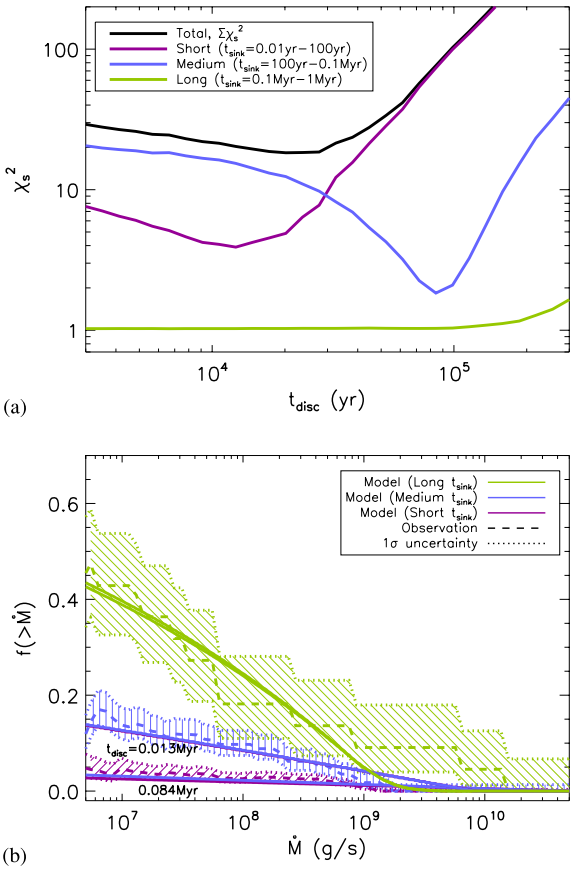


Figure 7. Simulations of accretion of 2.2×10^{22} g planetesimals at a mean rate 1.7×10^8 g s^{-1} that are identical to those for Fig. 5, except that sampling times combine both the sinking time in the white dwarf atmosphere and a disc lifetime ($t_{\rm disc}$). (a) Goodness-of-fit χ_s^2 as a function of disc lifetime for the different sinking time bins, as well as for all bins combined. (b) Comparison of the model populations to the rates inferred from observations for the disc lifetimes that provide the best fit to the short sinking time bin ($t_{\rm disc} = 0.013$ Myr) and to the medium sinking time bin ($t_{\rm disc} = 0.084$ Myr). For each of these disc lifetimes, the model populations in the medium and short sinking time bins are very similar and so are hard to differentiate. The model populations for the long sinking time bins are indistinguishable for the two disc lifetimes.

Downloaded from https://academic.oup.com/mnras/article/439/4/3371/1151716 by guest on 24 March 2022

requires $t_{\rm disc} \ll 0.01$ Myr, but that results in too few stars having accretion rates in the range of those inferred observationally. Since the accretion rate distributions inferred observationally for these bins differ at the 2–3σ level (Section 2.4), we consider that while this model with a disc lifetime in between 0.01 and 0.08 Myr would provide a reasonable fit to the observationally inferred distributions (e.g., if the medium and short sinking time bins were combined), this is mildly disfavoured by the observations. Thus, we continue to try to find a model that also predicts a difference between the short and medium sinking time bins.

4.3.2 Mono-mass, multirate with disc lifetime

To repeat the modelling for the case that the input accretion rates are not necessarily the same for all stars (i.e., modelling analogous to Section 4.2), it is helpful to note that the long sinking time bin must be unaffected by the disc lifetime, because otherwise the distributions for all sinking time bins would look the same. This means that the μ and σ of the distribution of input accretion rates required to fit the long bin can be taken from Fig. 6(a). Thus, these parameters were fixed (for a given $m_{\rm p}$), and the modelling was repeated for a range of $t_{\rm disc}$. For each disc lifetime, $m_{\rm p}$ was chosen so as to minimize χ_s^2 either of each of the sinking time bins, or of the total χ_s^2 for all bins.

Some general comments can be made on how the best-fitting parameters and the resulting accretion rate distributions vary with assumptions about disc lifetime. For $t_{\rm disc} \ll 1$ yr, the solution is unaffected by the disc lifetime, and the solution tends to that of Fig. 6. For $t_{\rm disc} \gg 0.1$ Myr, on the other hand, all bins have the same sampling time (i.e., close to the disc lifetime) and so all have the same distribution of inferred accretion rates. Since neither extreme provides a reasonable fit to the observationally inferred distributions, but for very different reasons – for small $t_{\rm disc}$, the distributions of the different bins are too far apart, whereas for large $t_{\rm disc}$ the distributions are too similar — it might be hoped that an intermediate value of $t_{\rm disc}$ would improve the fit. This is indeed the case; however, the improvement is very small, since an intermediate disc lifetime is the situation described in Section 4.3.1, and the problems of that model are not much ameliorated by allowing there to be a distribution of input accretion rates; that is, it is still not possible to separate the three sinking time bins.

Thus, we conclude that none of the mono-mass planetesimal distribution models provide an adequate fit to the observationally inferred accretion rate distributions, with the caveat that this requires those distributions for the three sinking time bins to be different from each other, which needs confirmation. The line of reasoning outlined above also suggests that if thermohaline convection modifies the rates such that these are independent of sinking time (see Section 2.5), this could be used to argue for a disc lifetime $\gg$0.1 Myr, in which case a mono-mass planetesimal distribution remains a possibility.

5 MODELS OF ACCRETION FROM PLANETESIMALS WITH A RANGE OF MASSES

In this section, we relax the assumption that the accreted material is all in planetesimals that are of the same mass (i.e., mono-mass), and instead assume that material is accreted at a mean rate $\dot{M}_{\rm in}$ from a power-law mass distribution that is defined by the index q. That is, if $n(m)\,{\rm d}m$ is the number of objects in the mass range m to $m + {\rm d}m$ then

$$n(m) \propto m^{-q}, \tag{16}$$

where this parametrization means that the commonly quoted index on the size distribution (i.e., $n(D) \propto D^{-\alpha}$) would be $\alpha = 3q - 2$ for spherical particles of constant density. If we assume that $q < 2$, and that the most massive planetesimal in the distribution, of mass $m_{\rm max}$, is much more massive than the least massive dust grain, of mass $m_{\rm min}$, then the majority of the mass is in the largest objects and the new model is simply defined by two parameters (q and $m_{\rm max}$) instead of one ($m_{\rm p}$). While one might imagine that this would be equivalent to a mono-mass distribution with mass $m_{\rm p} \sim m_{\rm max}$, this is not the case if the number of planetesimals with mass $m_{\rm max}$ arriving per sampling time (i.e., the larger of the sinking time and disc lifetime, equation 15) is less than unity. In Section 5.1, we show how the distribution of accretion rates that would be inferred is more closely related to planetesimals of mass $m_{\rm tr} < m_{\rm max}$ for which the total number of planetesimals with masses larger than $m_{\rm tr}$ arriving each sampling time is of the order of unity. Then in Section 5.2, we show that this model can be used to provide a reasonable fit to the observationally inferred distribution of accretion rates.

5.1 Simple model

To illustrate the effect of planetesimals having a distribution of masses, Fig. 8 shows the predictions of a Monte Carlo model of accretion from a distribution in which $q = 11/6$ and $m_{\rm max} = 3.16 \times 10^{22}$ g. To do this, $N_{\rm m} = 200$ logarithmically spaced mass bins were set up down to an inconsequentially small minimum mass of $m_{\rm min} = 10^7$ g. The logarithmic width of the bin is $\delta = (\log m_{\rm max} - \log m_{\rm min})/N_{\rm m}$, and bins are referred to by their index k, so that planetesimals in the bin have a typical mass denoted m_k. Assuming a mean accretion rate of $\dot{M}_{\rm in} = 10^{10}\,{\rm g\,s^{-1}}$, the amount of mass accreted from each bin in a given time interval, and the amount of mass that remains in the atmosphere from previous accretion events from that bin (for a given sampling time $t_{\rm samp}$), was then modelled in exactly the same way as described for the accretion of a mono-mass planetesimal distribution (Section 3.2). The results for all of the bins were then combined to get the expected distribution of mass in the atmosphere for the $N_{\rm tot} = 200\,000$ timesteps. This process was repeated for different sampling times in the range $t_{\rm samp} = 10^{-3}$ to 10^9 yr.

The snapshot shown in Fig. 8(a) illustrates how the accretion from different mass bins can be divided into a continuous and a stochastic component. For a given sampling time, for small enough planetesimal masses, the mass accreted from different bins simply follows the mass distribution, with mass accreted in the interval of duration $t_{\rm samp}$ being

$$M_{\rm ac(k)} = (2 - q)\dot{M}_{\rm in} t_{\rm samp} \delta (m_k/m_{\rm max})^{2-q}. \tag{17}$$

However, since only integer numbers of particles can be accreted in any one timestep, this relation breaks down for bins for which the mass that would have been expected to be accreted is comparable with that of a single planetesimal.

As noted in Section 3, what is important is the mean number of planetesimals accreted from bin k per sampling time, $M_{\rm ac(k)}/m_k$. However, to avoid having model parameters that depend on bin size δ, here we integrate equation (17) from $m_{\rm min}$ to m_k to get the mass accreted in $t_{\rm samp}$ from objects smaller than m_k. We then use this to work out the number of planetesimals of mass m_k that would need

Downloaded from https://academic.oup.com/mnras/article/439/4/3371/1151716 by guest on 24 March 2022

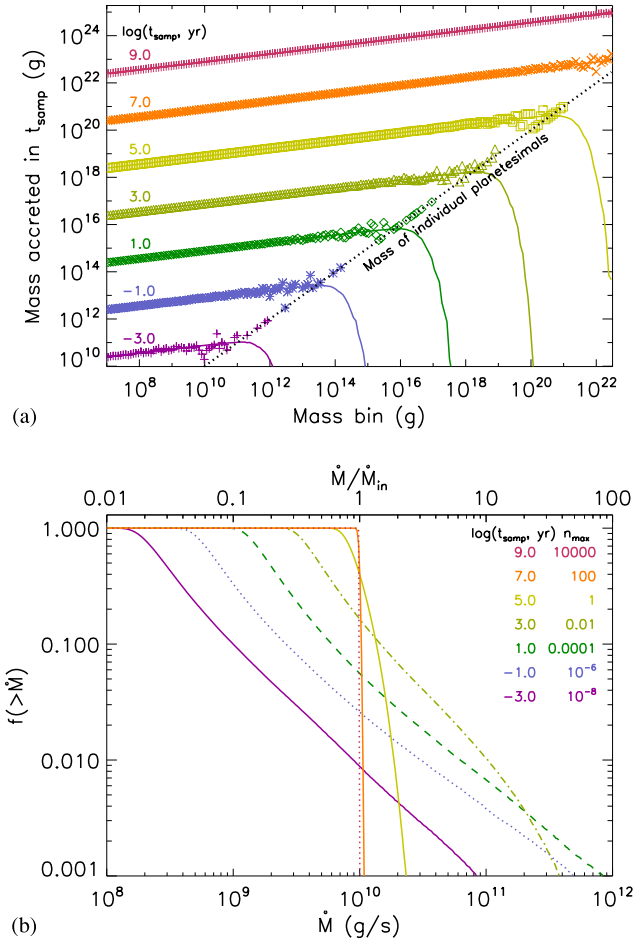


Figure 8. Monte Carlo simulations of sampling a mass distribution with $m_{\rm max} = 3.2 \times 10^{22}$ g and a power-law index $q = 11/6$ at a rate 10^{10} g s^{-1} with different sampling times $t_{\rm samp}$. (a) Snapshot of the mass accreted from different logarithmically spaced mass bins over a time interval of one sampling time (symbols), where models with different sampling times are shown with different colours. The solid coloured lines use the results of many snapshots to show the median mass remaining in the atmosphere from the accretion of material from this bin. (b) Distribution of accretion rates that would be inferred after many realizations of the snapshots seen in (a).

to be accreted per sampling time to maintain that accretion rate

$$n_k = n_{\rm max}(m_k/m_{\rm max})^{1-q}, \tag{18}$$

$$n_{\rm max} = \dot{M}_{\rm in} t_{\rm samp}/m_{\rm max}, \tag{19}$$

where $n_{\rm max}$ is the mean number of the largest planetesimals in the distribution that would need to be accreted to maintain the input accretion rate (if only those largest planetesimals were present).

The planetesimal mass at which $n_k = 1$, which we call

$$m_{\rm tr} = m_{\rm max} n_{\rm max}^{1/(q-1)}, \tag{20}$$

is that at which the mass accreted in $t_{\rm samp}$ from planetesimals less massive than $m_{\rm tr}$ is equal to a single planetesimal of mass $m_{\rm tr}$. This mass marks the transition from continuous to stochastic accretion; in any given timestep, most bins above $m_{\rm tr}$ would be expected to have no planetesimals accreted from them, with the occasional bin offering up the accretion of a single planetesimal. The solid lines on Fig. 8(a) show that the mass left in the atmosphere from such bins is, in an average timestep, very small. Thus, the typically inferred accretion rate is dominated by the accretion of objects of mass around $m_{\rm tr}$.

Fig. 8(b) shows the distribution of mass accretion rates that would be expected to be inferred, given the mass that would remain in the atmosphere for the given sampling times, for the $N_{\rm tot}$ realizations of the model. For long enough sampling times all planetesimal masses are accreted continuously and all timesteps measure an accretion rate equal to the mean rate of 10^{10} g s^{-1}. As a stochastic element only arises if $m_{\rm tr} < m_{\rm max}$, the sampling time above which stochasticity is unimportant can be estimated by setting $m_{\rm tr} = m_{\rm max}$ in equation 20, so that

$$t_{\rm samp,crit} = m_{\rm max}/\dot{M}_{\rm in}; \tag{21}$$

i.e., we would expect $t_{\rm samp,crit}$ to be 0.1 Myr for the parameters given here, in agreement with Fig. 8(b) for which the accretion rates are in a narrow distribution around 10^{10} g s^{-1} for $\log(t_{\rm samp}) \gg 5$.

For sampling times significantly below this value, however, we expect different timesteps to measure different accretion rates, depending on whether stochastic processes happen to have favoured the timestep (or those in the recent past) with many or few objects of mass around $m_{\rm tr}$ and above. As mentioned previously, the distribution must still have a mean of $\dot{M}_{\rm in}$. However, for short sampling times the mean would be dominated by events so rare (like the accretion of a planetesimal of mass $m_{\rm max}$) that it is unlikely to be measured in any of our timesteps for a realistic value of $N_{\rm tot}$. Nevertheless, our realizations give an indication of the median of the distribution, and so of the typical level of accretion that would be seen. It is notable that the median tends to smaller values for smaller sampling times.

To quantify the median accretion rate discussed above, Fig. 9(a) shows this as a function of $t_{\rm samp}$ for the model above (with $q = 11/6, m_{\rm max} = 3.16 \times 10^{22}$ g and $\dot{M}_{\rm in} = 10^{10}$ g s^{-1}), as well as for the same model but for accretion from mass distributions with different slopes q. Clearly, how the median accretion rate varies with sampling time is a strong function of that slope. To understand why, we apply a simple model in which the median accretion rate is approximated as that continuously accreted from objects smaller than $m_{\rm tr}$, which would result in

$$\dot{M}_{\rm med} = (m_{\rm max}/t_{\rm samp}) n_{\rm max}^{1/(q-1)}. \tag{22}$$

This equation would hold for $t_{\rm samp} < t_{\rm samp,crit}$, but for longer sampling times, the median accretion rate would be the mean accretion rate $\dot{M}_{\rm in}$. Despite its simplicity, Fig. 9(a) shows that this prescription fits the Monte Carlo model reasonably well. Thus, we consider that the effect of stochasticity on such accretion measurements is also well understood in the regime of accretion from a mass distribution, and that we can extrapolate the results presented here to arbitrary sampling times, mean accretion rates, maximum planetesimal masses and power-law indices, as indicated in the top and right axes of Fig. 9(a).

While Fig. 9(a) shows the median of the distribution, it does not describe its width, which is characterized in Fig. 9(b) using the range of accretion rates that cover the 90, 10 and 1 per cent points in the distribution. As was already evident from Fig. 8(b), as long as $t_{\rm samp} \ll t_{\rm samp,crit}$ (i.e., $n_{\rm max} \ll 1$), the width of this distribution is relatively constant and independent of $t_{\rm samp}$. However, the breadth of the distribution also depends on q, with steeper mass distribution slopes (larger q) resulting in narrower accretion rate distributions.

The predictions of the model for stochastic accretion from a mono-mass planetesimal distribution are also plotted on Fig. 9 (reproduced from Fig. 4 with appropriate scaling). This comparison shows that the incorporation of a distribution of masses for the

Downloaded from https://academic.oup.com/mnras/article/439/4/3371/1151716 by guest on 24 March 2022

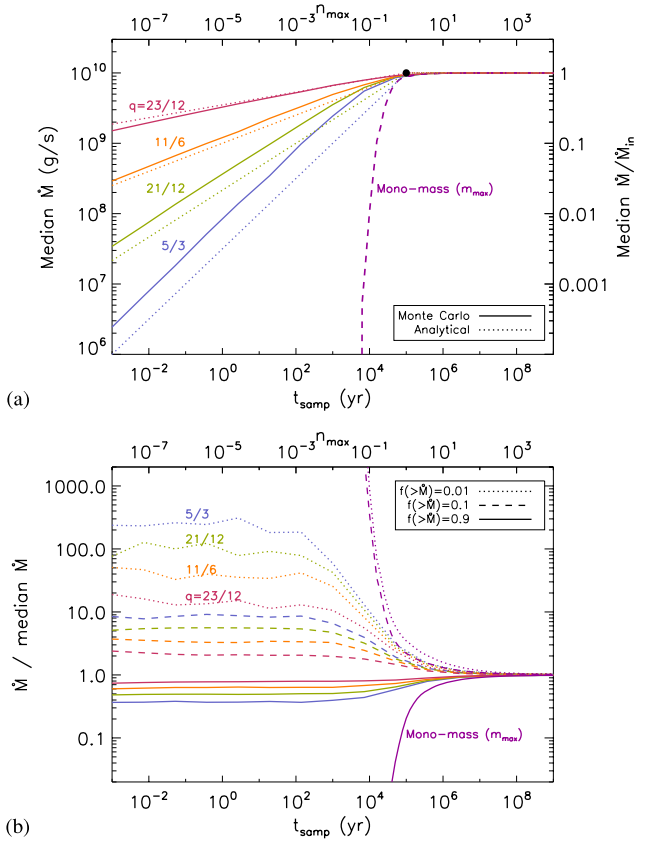


Figure 9. Monte Carlo simulations of sampling a mass distribution with $m_{\rm max} = 3.2 \times 10^{22}$ g and a power-law index q at a rate 10^{10} g s^{-1} with different sampling times $t_{\rm samp}$. (a) Median accretion rate as a function of $t_{\rm samp}$ for models with different mass distribution slopes q (indicated with different colours). The solid line is the result of the Monte Carlo models, and the dotted line is the analytical prediction of equation (22). The mono-mass model of Fig. 4 (appropriately scaled so that all planetesimals are of mass $m_{\rm max}$) is shown with a dashed line. (b) The width of the distribution of accretion rates, as defined by the accretion rates for which 90 per cent, 10 per cent and 1 per cent of measurements are expected to have values higher than this (relative to the median accretion rate).

accreted material substantially changes the character of the accretion rate distribution that would be measured. One difference is that the median accretion rate changes much more slowly with sampling time. This is because, for short sampling times, there is not only mass present in the atmosphere shortly after an accretion event, rather there is always mass in the atmosphere, albeit at a slightly lower level, from the accretion of small objects in the distribution. Another difference is that the accretion rate distribution is much narrower, because there is always a plentiful supply of small objects to maintain the mass in the atmosphere at a steady level, even if larger objects can still be accreted leading to increased mass levels.

5.2 Population model

Having characterized what the distribution looks like for a single accretion rate, it is relatively simple to determine what kind of population model would be needed to fit the data.

5.2.1 Constraint on $m_{\rm max}$, μ and σ

First of all, we can use the arguments of Section 4.1 to rule out the mono-rate model by looking at the long sinking time bin. This is because Fig. 9(b) shows that the factor of ∼1000 between the inferred accretion rate at the 10 per cent and 50 per cent points in the distribution cannot be achieved without a mass distribution with a very small value of q. This would be equivalent to having a mono-mass distribution, which was ruled out from the shorter sinking time bins in Section 4.1. Thus, as in Section 4.2, we assume a log-normal distribution for $\dot{M}_{\rm in}$ parametrized by μ and σ.

The distribution of accretion rates in the long sinking time bin is not indicative of the shape of the mass distribution, rather it is more likely representative of the distribution of input accretion rates (as surmised in Section 4.2). The correspondence is not necessarily exact, as the input accretion rates could be higher than this. Indeed, if the maximum planetesimal mass was large enough so that $n_{\rm max} < 1$ for $t_{\rm sink} \approx 1$ Myr and $\dot{M}_{\rm in} \approx 10^{10}$ g s^{-1}, then the accretion rates would on average be inferred to be lower than the input rates for all stars in this bin (and for all stars in all bins); this corresponds to a maximum planetesimal mass of $>3.2 \times 10^{23}$ g. While Section 4.2 used this argument to set an upper limit on $m_{\rm p}$ that is even lower than this, such a constraint is not necessary here. This is because, although the distribution of inferred rates would be broader than that of the input rates when $n_{\rm max} < 1$, the mass distribution limits the effect of broadening to a level that depends on q (Fig. 9 b), and it is only extremely small values of q (i.e., mono-mass distributions) for which that broadening is so great that it is required that $n_{\rm max} > 1$ to curtail it.

In fact, it turns out to be necessary in this instance for the maximum planetesimal mass to be larger than the limit given in the last paragraph. If it were much lower than this, then it would still be possible to construct an input accretion rate distribution that allows a reasonable fit to the long sinking time bin (e.g., for small enough $m_{\rm max}$ this would be $\mu = 6.6$ and $\sigma = 1.5$ as discussed in Section 4.2). However, a significant fraction of the white dwarfs in the shorter sinking time bins would have $n_{\rm max} > 1$ and so would have inferred accretion rates that are indistinguishable from those in the long sinking time bin. This issue is just becoming evident in Fig. 6(c), where the model distributions for the long and medium sinking time bins are indistinguishable for $\dot{M} > 10^9$ g s^{-1}.

On the other hand, as long as $m_{\rm max}$ is above this limit, then its value does not affect the quality of the fit. This is because, as long as $n_{\rm max} \ll 1$ for all white dwarfs, the distribution of accretion rates measured on each is the same if $\dot{M}_{\rm in} m_{\rm max}^{q-2}$ is kept constant (see equation 22 and Fig. 9). That is, if we increase $m_{\rm max}$ above this limit, we can ensure that the model retains the same accretion rate distributions for the different sinking time bins by also increasing μ proportionately. Thus, we will set $m_{\rm max} = 3.2 \times 10^{24}$ g, i.e., a factor of 10 above this limit, which is comparable with the mass of the largest Kuiper belt objects, noting that lower values may be possible, as long as they are accompanied by lower input accretion rates, though we expect the fit to the shorter sinking time bins to deteriorate as $m_{\rm max}$ is decreased.

Note that another consequence of all white dwarfs accreting with $n_{\rm max} < 1$ is that the distributions of observationally inferred accretion rates should have very similar shapes for the different sinking time bins. It is just their median levels that would be offset by an amount that can be estimated from equation (22)

$$\dot{M}_{\rm med} \propto t_{\rm samp,med}^{(2-q)/(q-1)}, \qquad (23)$$

where $t_{\rm samp,med}$ is the median sampling time in the bin. This is true as long as this width is not dictated by the width of sampling times within the bin, since this means that the bins have the same width in their distribution of $n_{\rm max}$.

Downloaded from https://academic.oup.com/mnras/article/439/4/3371/1151716 by guest on 24 March 2022

Practically we proceed with the modelling by assuming a value for q (and for $m_{\rm max}$), and then constraining the parameters of the input accretion rate distribution μ and σ from a fit to the long sinking time bin.

5.2.2 *Constraint on q and $t_{\rm disc}$*

Given that the input accretion rate distribution can be chosen to provide a reasonable fit to the long sinking time bin, the shorter sinking time bins can be used consecutively to determine the parameters q and $t_{\rm disc}$. For example, the medium sinking time bin has the 15 per cent point in its distribution a factor of $R_{\dot{M}} \approx 0.036$ lower in accretion rate than that of the long bin. Since the median sinking times of these bins are 850 yr and 0.37 Myr and so have a ratio $R_{\rm t} = 0.0024$, then equation (23) shows that, ignoring any effect of disc lifetime, this would require

$$q = (2 + X_{\rm R})/(1 + X_{\rm R}), \tag{24}$$

where $X_{\rm R} = \log R_{\dot{M}} / \log R_{\rm t} \approx 0.56$. That is, to get a simultaneous fit to these bins would imply $q \approx 1.64$.

The problem is that the same argument cannot apply to the short sinking time bin, since the median sinking time in this bin is 0.017 yr, which is $R_{\rm t} = 4.7 \times 10^{-8}$ lower than that of the long bin, which means that its accretion rate distribution should be $\sim 10^{-5}$ times lower than that of the long bin. Although the paucity of detections in the short sinking time bin (due to the poorer detection threshold for these white dwarfs that are necessarily younger and hotter) means that its distribution is not well known, the fact that there are any detections at all seems to rule this out. However, the distribution inferred from the observations is readily accounted for if the accretion is mediated through a disc as discussed in Section 4.3, since this would increase the effective sampling time (equation 15), exclusively in the short bin for a suitably chosen disc lifetime. Given that the inferred accretion rate distribution is poorly defined observationally, any estimate of the disc lifetime on this basis would have significant uncertainty. To make progress, we note that the different sinking time bins should have distributions that are offset in accretion rate by a factor of around $t_{\rm samp}^{X_{\rm R}}$ (see equation 23). Thus, to get the 5 per cent points in the short and long sinking time bins offset by $\sim 10^{-3}$ would require the short bin to have a median sampling time of around 2 yr.

Combining these previous estimates, and making small (consecutive) adjustments to improve the fit, we show in Fig. 10 the predictions for a population model with the following parameters: $m_{\rm max} = 3.2 \times 10^{24}$ g, $\mu = 8.0, \sigma = 1.3, q = 1.57, t_{\rm disc} = 20$ yr. Given the arguments in the preceding paragraphs, it is not surprising that this provides a reasonable qualitative fit to the observationally inferred accretion rate distributions, including how those distributions differ between the sinking time bins. Quantitatively the fit is also good, with $\chi_s^2 = 0.8, 2.9, 1.7$ for the long, medium and short sinking time bins, respectively. We prefer not to give formal uncertainties on the model parameters, since this gives the impression that they are better constrained than they really are, and ignores the (still quite significant) uncertainty in the rate distributions inferred from the observations, as well as the systematic uncertainty on whether the model includes all of the relevant physics. Rather the intention here is to show how the model behaves, to show that it provides a qualitatively reasonable fit to the observationally inferred accretion rate distributions, and to motivate further observations that provide better constraints on these distributions, and their dependence on sinking time and cooling age. Nevertheless, the discussion above illustrates the various degeneracies between the different parameters,

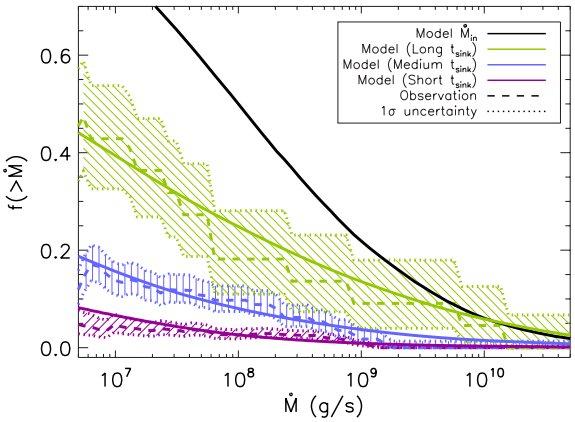


Figure 10. Population model fit to the observationally inferred accretion rate distributions for a model in which the accreted material has a mass distribution defined by $m_{\rm max} = 3.2 \times 10^{24}$ g and $q = 1.57$, the input accretion rates have a log-normal distribution defined by $\mu = 8.0$ and $\sigma = 1.3$, and a disc lifetime of $t_{\rm disc} = 20$ yr was also assumed.

and also gives a feeling for how changing these parameters would affect the quality of the fit.

6 DISCUSSION

Thus far, we have discussed how the stochastic accretion of a mono-mass planetesimal distribution would be manifested in observations of white dwarfs with different sinking times (Section 3), as well as the effect of allowing the mass distribution to encompass a range of masses (Section 5.1). These models were then compared with observations of metal pollution on to white dwarfs that were used to get inferred accretion rate distributions as summarized in Section 2. It was shown that, although the mono-mass distribution can provide a reasonable fit to these distributions, it does not reproduce the correct qualitative differences with sinking time (Section 4), while allowing a mass distribution results in a much better fit and the correct qualitative behaviour (Section 5.2). This section considers the implications of the model results. To start with, in Section 6.1 we outline a physical picture for the evolution of the material that is accreted by the white dwarfs. In Section 6.2, we consider how the parameters derived in the previous sections fit in with that picture. We also consider caveats to the model, and how it might need to be improved upon in the future (Section 6.3), as well as observational avenues to further constrain what is going on (Section 6.4).

6.1 Physical model of accretion on to white dwarfs

Consider that the main-sequence progenitor of the white dwarf had an orbiting belt of planetesimals, like the Solar system's asteroid or Kuiper belts. If their orbits were stable for at least several hundred Myr this belt would have survived to the post-main sequence (e.g., Greenstein 1974). Unless the belt is very low mass, and assuming the collision velocity is high enough (Heng & Tremaine 2010), it is inevitable that mutual collisions amongst the planetesimals would have set up a collisional cascade. While this would have reduced the belt mass, it also means that its mass distribution would be reasonably well defined. For example, for the ideal case where the planetesimals' dispersal threshold is independent of mass it would be expected that $q = 11/6$. For the more realistic case that the dispersal threshold is mass dependent, this would result in a distribution with a slightly different index, or one in which the

Downloaded from https://academic.oup.com/mnras/article/439/4/3371/1151716 by guest on 24 March 2022

distribution exhibits different indices in different mass ranges (e.g., O'Brien & Greenberg 2003; Wyatt, Clarke & Booth 2011).

When the star evolved to become a white dwarf, some mechanism could perturb the orbits so that material is scattered from the belt towards the star. Like the comets in the Solar system, some of this material would end up being accreted on to planets or ejected into interstellar space or scattered into an Oort Cloud analogue. However, some fraction could end up incorporated into a disc that accretes on to the star. One candidate for the perturbing process is that the inner edge of the belt was located at the edge of the chaotic region of resonance overlap of an interior planet, and that stellar mass-loss caused the size of that unstable region to expand (Bonsor, Mustill & Wyatt 2011). Another possibility is that a planet lies exterior to the belt, and that one of its resonances lies in the middle of the belt; the resonance is unstable, and so empty on the main sequence (similar to the Kirkwood gaps in the asteroid belt), but stellar mass-loss causes the resonance to expand feeding mass into the dynamically unstable region (Debes, Walsh & Stark 2012).

Both of the mechanisms discussed above are dynamical and affect all material in the belt regardless of mass. This means that the mass that is scattered would retain the mass distribution of the belt, and it might be expected that the mass distribution of accreted material (i.e., that described in equation 16) is indicative of the mass distribution of the belt. However, there are physical processes that might bias the scattering process to different masses; e.g. sub-km planetesimals could have been dragged in by stellar wind drag during the AGB phase (Bonsor & Wyatt 2010), perhaps also getting trapped in planetary resonances as a result (Dong et al. 2010). The efficiency of tidal disruption, or of subsequent incorporation into a disc, may also have some dependence on the mass of the original object, so that the mass distribution of accreted material may differ from that of the belt.

6.2 Implications of model fits

Given the physical picture of Section 6.1, we can now discuss whether the model parameters required to fit the observationally inferred accretion rate distributions (i.e., those given in Section 5.2) are physically plausible.

Accretion rate distribution (μ and σ). The inferred accretion rate distribution is remarkably similar to that derived in the model of Bonsor et al. (2011). That model used the well-characterized population of main-sequence A star debris discs (Wyatt et al. 2007), determined what that population would look like at the start of the white dwarf phase (Bonsor & Wyatt 2010), then considered the fraction of mass scattered due to the increase of resonance overlap due to stellar mass-loss if the discs were truncated at the inner edge by a planet. A fixed fraction of the scattered mass (0.6 per cent based on simulations of the Solar system) was assumed to make it on to the star, and figs 7–8 of their paper predict the distribution of mass accretion rates experienced by white dwarfs as a function of age. Here, we fit the Bonsor et al. (2011) results with log-normal distributions to get the appropriate μ and σ at different ages. We find that white dwarfs in the age range 10–5000 Myr in their model have an approximately log-normal distribution of accretion rates with $\mu = 8.1$ and $\sigma = 1.6$, coincidentally almost identical to that in our model. There is a slight dependence on age in their model, in that the median decreases $\propto t_{\rm age}^{-1.1}$, though we show in Section 6.3 that this is still consistent with the observationally inferred accretion rates in Section 2.4. While the agreement with our results should not be taken as strong support for the Bonsor et al. (2011) model – indeed the other models for the origin of the accretion (e.g., Debes et al. 2012) may reproduce a similar distribution of accretion rates – it does at least mean that the required rates are at a level, and have a width in their distribution, that is physically plausible.

Mass distribution ($m_{\rm max}$ and q). The mass distribution required to fit the observationally inferred accretion rate distributions is in-line with the distribution expected for the parent belt due to collisional evolution. Although $q = 11/6$ is that expected in an infinite cascade of planetesimals with dispersal threshold that is independent on mass (Dohnanyi 1969), it is expected that planetesimals more massive than 10^{12} g have strengths that increase with mass, i.e. $Q_{\rm D}^\star \propto m^b$, due to self-gravity so that $q = (11 + 3b)/(6 + 3b)$ (O'Brien & Greenberg 2003; Wyatt et al. 2011). Typically, $b \approx 1/2$ in this regime giving $q \approx 5/3$ (e.g., Benz & Asphaug 1999; Löhne, Krivov & Rodmann 2008). This is a reasonable approximation for the asteroid belt, which is thought to have reached collisional equilibrium, at least for objects smaller than around 3×10^{21} g, before it was depleted to its currently low level (e.g., Durda, Greenberg & Jedicke 1998; Bottke et al. 2005). However, the mass distribution in the Kuiper belt is weighted more to smaller objects (see Vitense, Krivov & Löhne 2010), likely because it retains the primordial distribution; this is closer to the distribution with $q = 2$ assumed in the models of Jura (2008). Thus, one implication of the low value of $q = 1.57$ inferred here could be that the accretion on to white dwarfs originates in a collisionally evolved population. This is perhaps unsurprising, since this only rules out planetesimal belts that are very far from the star (for which collisional evolution time-scales are long), or those that were depleted in dynamical instabilities, both of which might be expected to be unfavourable to high accretion rates. However, it is not clear that q in this model corresponds exactly with that in the parent belt, since some mass ranges could be more readily incorporated into an accretion disc.

Having constrained the mass distribution it is also helpful to remind the reader that in the model most stars are accreting continuously from objects in the mass distribution up to a mass $m_{\rm tr}$. Although that mass varies from star to star, it is possible to obtain a feeling for what objects are contributing to the observations by considering that the model's behaviour can be well explained by assuming that the accretion rate that is inferred for a given star is its median level, which is $m_{\rm tr}/t_{\rm samp}$ (see equation 22). This means that, perhaps unsurprisingly, $m_{\rm tr} = \dot{M}_{\rm obs} t_{\rm samp}$ and so is usually roughly the mass in pollutants in the white dwarf's convection zone (except for the DAs with sinking times that are shorter than the disc lifetime). So, for commonly inferred accretion rates of around 10^8 g s^{-1}, such accretion levels for a typical star in the long sinking time bin (i.e., one with the median sampling time of 0.37 Myr), would be dominated by the accretion of 1.2×10^{21} g objects, those in the medium bin (with a median sampling time of 850 yr) by 2.7×10^{18} g objects, and those in the short bin (with a median sampling time of 20 yr set by the disc lifetime) by 6.3×10^{16} g objects; these values correspond to 91, 12 and 3.4 km diameter objects, respectively, for a density of 3 g cm^{-3}. However, note that since inferred accretion rates span roughly four orders of magnitude, with a similar range in sampling times, these values should only be considered representative for each bin. Considering the polluted DAs in our sample, we find that $m_{\rm tr}$ covers the range 2.3×10^{15} to 7.1×10^{19} g (with a median of 5.2×10^{17} g), while that for polluted non-DAs covers the range 6.2×10^{19} to 1.3×10^{23} g (with a median of 9.6×10^{20} g). This means that there is a continuous range of $m_{\rm tr}$ spanning eight orders of magnitude in mass, but that the planetesimals dominating the pollution on DAs and non-DAs are smaller and larger, respectively, than $\sim 6.6 \times 10^{19}$ g (i.e., $\sim$35 km diameter for 3 g cm^{-3}).

Downloaded from https://academic.oup.com/mnras/article/439/4/3371/1151716 by guest on 24 March 2022

To understand why there is (coincidentally) such a neat division between DAs and non-DAs, it is helpful to note that lines of constant $m_{\rm tr}$ are horizontal on Fig. 2(c) up to $t_{\rm sink} = t_{\rm disc}$ (i.e., 20 yr in our best-fitting model), then fall off $\propto t_{\rm sink}^{-1}$ for $t_{\rm sink} > t_{\rm disc}$.

Similar logic can be used to estimate the input accretion rate as

$$\dot{M}_{\rm in}/\dot{M}_{\rm obs} = (\dot{M}_{\rm obs} t_{\rm samp}/m_{\rm max})^{q-2}, \quad (25)$$

where the quantity in parentheses is the number of objects of mass $m_{\rm max}$ that would have to be accreted per sampling time to reproduce the inferred rate. To give a couple of specific examples:

(i) The $\sim 10^{21}$ g of metals in the atmosphere of the prototypically polluted non-DA white dwarf vMa2, that has a sinking time of $\sim$3 Myr, gives an inferred accretion rate of $\sim 10^{7}$ g s^{-1}. In this model, equation (25) says that the input accretion rate is likely to be around 30 times higher than that inferred from the observations, which would put it slightly above the median input rate in the model; the pollutants currently in the atmosphere arrived in multiple accretion events of planetesimals smaller than $\sim$84 km.

(ii) The 10^{16} g of metals in the atmosphere of the prototypical DA white dwarf G29-38, that has a sinking time of <1 yr, gives a higher than average inferred accretion rate of $\sim 10^{9}$ g s^{-1}. Equation (25) implies that this star has a much higher than average input accretion rate of $\sim 6 \times 10^{11}$ g s^{-1}, which would put it in the top 0.2 per cent of accretion rates, and its pollutants arrived in multiple accretion events of $\leq$6 km planetesimals. Note that accretion levels above 10^{9} g s^{-1} in the short sinking time bin occur around just $0.8^{+0.6}_{-0.4}$ per cent of the sample, both in the distributions inferred observationally and in the model, consistent with the above consideration of the rarity of this object.

Disc lifetime. As discussed in Section 5.2, the constraints on the disc lifetime are not very stringent. We know that it must be shorter than $\sim$0.1 Myr for there to be a dependence on sinking time (since otherwise all stars would have the same sampling time irrespective of their sinking time), and further that it must be shorter than around 1000 yr if we want there to be a difference between the two shorter sinking time bins. A disc lifetime as short as 20 yr, if confirmed in later analysis, would have significant implications for the physics of the disc accretion, but we do not discuss this further here given the simple way in which disc lifetime was included in this model, and that any statement on the disc lifetime should also take into account observational evidence concerning the disc itself (e.g., regarding near-IR excesses or gas).

It should be noted that a disc lifetime of 20 yr does not necessarily mean that pollution levels are expected to decay on such time-scales. While the signature of individual events would decay on the sampling time-scale (equation 15), the pollution levels of many stars in this model are maintained indefinitely from multiple accretion events (although individual events can result in temporarily higher levels). To quantify this, Fig. 11 shows the predicted evolution of the accretion signatures for 20 stars from the best-fitting model population of Fig. 10 that fit the characteristics of G29-38, that is currently inferred to be accreting at a rate of 10^{9} g s^{-1} and has a sinking time of <1 yr. This illustrates how for many stars like G29-38 the accretion is maintained at a similar level over decadal time-scales (consistent with the decades-long persistence of circumstellar dust and pollution towards G29-38: Zuckerman & Becklin 1987; Koester, Provencal & Shipman 1997; Hoard et al. 2013), but that a rare few will undergo further brightening events, while a larger fraction will decay monotonically over the disc time-scale. A similar plot for vMa2, for which pollution in its atmosphere has persisted for around a century (van Maanen 1917; Dufour et al. 2007), predicts

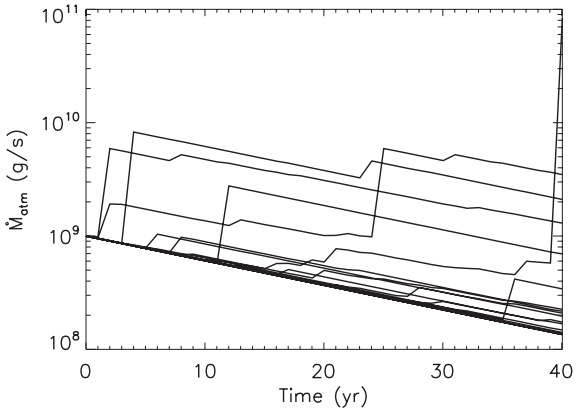


Figure 11. Evolution of the inferred accretion rate for 20 stars from the model of Fig. 10 that fit the characteristics of G29-38 ($t_{\rm sink} \approx 1$ yr and $\dot{M}_{\rm atm} = 10^{9}$ g s^{-1} at the present day).

no discernable evolution on such time-scales due to the $\sim$3 Myr sinking time for this non-DA star.

Since the disc time-scale is not well constrained in this model, we note that monitoring variability in accretion signatures on DA white dwarfs would be an excellent way to set constraints on this parameter. Variability in the accretion has been suggested for G29-38 based on a 70 per cent increase in atmospheric pollution over a two year time-scale (von Hippel & Thompson 2007), though other studies found the pollution level to have remained constant over time-scales of days to years (Debes & López-Morales 2008), and mid-IR observations of the circumstellar disc have also been shown to remain constant over yearly time-scales (Reach et al. 2009). Since 18/20 models on Fig. 11 remain within a factor of 2 of 10^{9} g s^{-1} over the first decade, but 3/20 undergo moderate levels of brightening (10–200 per cent increases) in this period, we conclude that the model is consistent with the observations.

6.3 Caveats

Several assumptions are implicit in the model, and were included not necessarily because these are the most physically realistic, rather to minimize model parameters that would be impossible to constrain.

We assumed that the accretion rate is constant and independent of age, justified by the lack of evidence for any age dependence in the observationally inferred accretion rates. However, in Section 6.2 we noted that one of the physical models, and perhaps all of them (e.g., Veras et al. 2013), require some fall-off with age. It would be relatively simple to include an age dependence in the model; for example, the model population could have both the same sinking time distribution and the same cooling age distribution as the observed population. One consequence of this would likely be that we would infer a steeper slope (higher q) for the mass distribution. This is because of the point noted at the end of Section 2.4 that a decrease in accretion rate with age would mean that the accretion rate distribution in the medium sinking time bin would have been higher relative to the other two bins had it been measured at a comparable age.

It should also be possible to use the lack of age dependence in the observationally inferred accretion rates to set constraints on the evolution of the input accretion rate. For example, the Bonsor et al. (2011) model results in a median input accretion rate that decreases by a factor of 0.16 between cooling age bins of 100–500 Myr and 500–5000 Myr. Equation (22) shows that, for the inferred mass

Downloaded from https://academic.oup.com/mnras/article/439/4/3371/1151716 by guest on 24 March 2022

distribution index q, the consequence for the distribution of accretion rates would be to shift those in the older bin to lower values by a factor of $0.16^{1/(q-1)} \approx 0.04$. However, the same equation shows that this difference is counteracted by the 37 times higher median sampling time in the older cooling age bin (730 yr compared with 20 yr in the younger bin), which would be expected to increase this by $37^{(2-q)/(q-1)} \approx 15$. In other words, the net result would be for the older bin to appear to have accretion rates that are very similar to those in the younger bin, in agreement with Fig. 2(b). The low significance trend in Fig. 2(b) could argue against an evolution in accretion rates that is significantly faster than that of the Bonsor et al. (2011) model, but we consider that interpretation of any evolutionary signal is complicated by the sinking time dependence and so no strong statements can be made at this stage.

The mass distribution was assumed to extend up to objects nearly as massive as Pluto for all stars, and to have a single slope across all masses. The large value of $m_{\rm max}$ is not necessarily a problem, given the prevalence of debris discs. However, it should be noted that there is no requirement for objects larger than a few km in most debris discs (e.g., Wyatt & Dent 2002), though the presence of objects the mass of Pluto would provide a natural explanation for the origin of the disc stirring (Kenyon & Bromley 2004). Nevertheless, there remains a discontinuity between the parameters derived here and the model of Bonsor et al. (2011), which was itself based on a model in which the maximum planetesimal size was nominally 2 km and the distribution had a slope of $q = 11/6$ (Bonsor & Wyatt 2010). However, it should be noted that the Bonsor & Wyatt (2010) model parameters are only meant to be representative values, given its simplistic prescription for collisional evolution, and that more realistic models for collisional evolution on the main sequence would be expected to provide similar results for larger maximum planetesimal masses and with shallower slopes in the relevant regime (e.g., Löhne et al. 2008). Certainly future models could readily include a mass-dependent planetesimal strength (e.g., Wyatt et al. 2011), and the results incorporated into the Bonsor et al. (2011) model to make a revised prediction, though we would not anticipate the conclusions of this paper to be affected in any substantial way.

The implicit assumption that disc lifetime is independent of the accretion rate, of the mass of objects being accreted, and of disc mass, is more of a concern. If discs last longer when the accretion rate is larger, for example because it takes longer to break down large objects into dust, this would bias the observations towards detecting the most massive events (and vice versa). This is not a topic that we can cover adequately here, so we leave it for a future paper.

Another factor of concern noted in Section 2.5 is the uncertainty in the observationally inferred accretion rates, and in particular whether unmodelled processes that act on the material after it has been accreted, such as thermohaline convection in the stellar interior, would change the inferred accretion rates enough to come to different conclusions on how their distribution depends on sinking time. Assuming it is possible to approximate the signature of an accreted planetesimal in a white dwarf atmosphere with exponential decay (equation 2), albeit with a sinking time modified from that of gravitational settling, then the model presented here will still apply, and the implications of revised inferred accretion rate distributions can be understood within the context of the arguments in this paper. For example, as mentioned in Section 4.3.2, if the inferred accretion rate distributions turn out to be independent of (effective) sinking time, this would argue for a disc lifetime $\gg$0.1 Myr, effectively negating the importance of sinking time on how accretion is measured. This would mean that information on the mass distribution of accreted material cannot be gleaned from the inferred accretion rate distributions.

6.4 Future observations

One of the conclusions to arise from this analysis is to emphasize to observers that non-detections have equal value to detections in our interpretation of this phenomenon. That is, we urge that future observations are presented as the distribution of inferred accretion rates, and that these observations seek to quantify how those distributions vary with sinking time, and to search for evidence of a dependence on cooling age. It is premature to claim that the model can make testable predictions. Although Fig. 10 does make a prediction for how the accretion rate distributions extend to lower accretion levels, it should be recognized that the model has sufficient free parameters to fit other distributions should they arise from the observations, so a poor fit cannot be used to rule the model out. Rather, what we do claim is that a dependence of the inferred accretion rate distribution on sinking time is a natural consequence of the stochastic nature of accretion processes, and that we can learn about the mass distribution of accreted material, and also about the disc lifetime, by constraining those distributions through observations. For example, confirming that the accretion rate distributions exhibit progressively lower rates for shorter sinking times, with differences that are much smaller than the many orders of magnitude difference in sinking times, would strengthen the conclusion that the accretion arises from planetesimals with a wide range of masses, rather than from a mono-mass planetesimal distribution. Observations of the variability of accretion signatures on individual DA white dwarfs can also be informative of the disc lifetime (see Fig. 11).

Another promising avenue for comparison of the model with observations is to consider its compatibility with the fraction of stars with detectable accretion that have infrared excess. For example, 10/21 DA white dwarfs with accretion rates inferred at $>10^8$ g s^{-1} have infrared excess, whereas this fraction is lower at 7/30 for DB white dwarfs (Girven et al. 2012). This fits qualitatively within the context of the model presented here. Given the short lifetime of the disc, its luminosity would be expected to be set by the accretion of planetesimals in a similar mass range to those that dominate the atmospheric pollution of stars in the short sinking time bin. It is a relatively small fraction of the DAs that have accretion rates inferred to be $>10^8$ g s^{-1}, and those that do are likely to be those that have atypically large input accretion rates, and so it might be expected that these also have bright discs. However, it is a relatively large fraction of the DBs that have accretion rates inferred at this level, and so their input accretion rates would be expected to span a lower range than the DAs detected at this level, which would explain why their discs are fainter on average. Although this is qualitatively reasonable, such comparisons should be made more quantitatively along with a more detailed consideration of the observations, and a more detailed prescription for the disc in the model.

It might appear that one way of testing this model would be to use the observationally inferred accretion rates of different metals in the same star, since different metals have different sinking time-scales; e.g., this model would predict that metals with longer sinking time-scales originate in the accretion of (on average) more massive objects and so should exhibit a higher inferred accretion rate. However, Fig. 2(a) shows that sinking times vary only by a factor of a few for different metals. Furthermore, this analysis would only be appropriate if the abundance of the material being accreted was known, since otherwise differences could be explained by compositional variations. Thus, observations of different metals

Downloaded from https://academic.oup.com/mnras/article/439/4/3371/1151716 by guest on 24 March 2022

in the same star are usually used to determine the abundance of the accreted material, rather than to make inferences about the accretion process. However, Montgomery, Thompson & von Hippel (2008) show how measuring different variability patterns in the accretion rates of different metals could be used to set constraints on gravitational settling times.

7 CONCLUSION

This paper explores the effect of stochastic processes on measurements of accretion of planetesimals on to white dwarfs. We first quantified the distribution of accretion rates inferred from observations of atmospheric pollution in Section 2. As previous authors had found, we concluded that this distribution has a dependence on the time-scale for metals to sink in the atmosphere, with tentative evidence that our sample could be split into three sinking time bins with accretion rates that are progressively lower as sinking time is reduced; there was no evidence for a dependence on cooling age. These conclusions use the typical assumption that gravitational settling is the dominant process removing metals from the atmosphere. As such they should be revisited once the effect of thermohaline convection has been fully characterized.

In Section 3, we showed how the accretion of a mono-mass population of planetesimals would be manifested in observations of atmospheric pollution. We described the resulting distribution of inferred accretion rates both analytically and using a Monte Carlo model, demonstrating how stochastic processes cause that distribution to have a strong dependence on sinking time. We compared this model to the observationally inferred accretion rate distributions in Section 4 to find that while it is easy to reproduce the distributions inferred for one (or with more effort two) of the sinking time bins, a concurrent fit to the distributions in all three sinking time bins is not possible. The problem is that the many orders of magnitude difference in sinking time between white dwarfs would cause this model to have larger differences in inferred accretion rates than determined from the observations. The model of this ilk that most closely matches the observationally inferred distributions invoked a disc lifetime of 0.01–0.1 Myr to smooth out the accretion that is measured on stars with short sinking times.

In Section 5, we showed how allowing the accreted planetesimals to have a range of masses substantially changes the accretion rate distribution that would be inferred, with a less dramatic dependence of inferred accretion rates on sinking time more in-line with the observationally inferred accretion rates. There is also an important conceptual difference. With a mono-mass planetesimal distribution, stars only exhibit accretion signatures shortly after a planetesimal has been accreted. However, when there is a distribution of planetesimal masses, stars always exhibit accretion signatures, because small enough planetesimals (quantified in equation 20) are being accreted continuously. We show that such a model provides a good fit to the observationally inferred distributions with a relatively shallow mass distribution for the accreted material ($q = 1.57$), similar to that expected for a collisionally evolved population. Along with the other parameters of the model (e.g., the input accretion rate distribution), we find that the atmospheric pollution signatures are consistent with the accretion of the descendants of the debris discs seen around main-sequence stars, as predicted by Bonsor et al. (2011). There are however several outstanding questions, such as the origin and nature of the disc through which the accretion takes place.

If this interpretation is backed up with future observations, including a consideration of the importance of thermohaline convection on the inferred accretion rates, one implication is that atmospheric pollution does not always originate in the stochastic accretion of individual objects; i.e., pollution in non-DA white dwarfs is not necessarily a historical relic of past events (Farihi et al. 2012b). While the accretion of individual objects can affect the accretion signature, for many stars this is dominated by the continuous accretion of moderately sized planetesimals. The closest model in the literature to that presented here is the two population model of Jura (2008), in which large objects are accreted infrequently and small objects are accreted continuously. However, the role of stochastic processes is more subtle than suggested by that model, since the transition between these two populations occurs at different planetesimal masses for different stars, and this is what imprints the mass distribution on the distribution of observationally inferred accretion rates.

Finally, we note that the insight gleaned from this study into the way stochastic processes are manifested in observations may also relevant to other fields of astrophysics. For example, the origin of exozodiacal emission from the scattering of cometary material into the inner regions of nearby planetary systems is a process that has many analogies to that studied here (Bonsor, Augereau & Thebault 2012).

ACKNOWLEDGEMENTS

MCW acknowledges the support of the European Union through ERC grant number 279973. JF acknowledges support from the STFC via an Ernest Rutherford Fellowship.

REFERENCES

Althaus L. G., Córsico A. H., Isern J., García-Berro E., 2010, A&AR, 18, 471
Benz W., Asphaug E., 1999, Icarus, 142, 5
Bergeron P. et al., 2011, ApJ, 737, 28
Bilikova J., Chu Y.-H., Gruendl R. A., Su K. Y. L., De Marco O., 2012, ApJS, 200, 35
Bonsor A., Wyatt M. C., 2010, MNRAS, 409, 1631
Bonsor A., Mustill A. J., Wyatt M. C., 2011, MNRAS, 414, 930
Bonsor A., Augereau J.-C., Thebault P., 2012, A&A, 548, A104
Bonsor A., Kennedy G. M., Crepp J. R., Johnson J. A., Wyatt M. C., Sibthorpe B., Su K. Y. L., 2013, MNRAS, 431, 3025
Bottke W. F., Durda D. D., Nesvorný D., Jedicke R., Morbidelli A., Vokrouhlický D., Levison H., 2005, Icarus, 175, 111
Brown J. M., Garaud P., Stellmach S., 2013, ApJ, 768, 34
Campbell N., 1909a, Proc. Camb. Phil. Soc., 15, 117
Campbell N., 1909b, Proc. Camb. Phil. Soc., 15, 310
Chu Y.-H. et al., 2011, AJ, 142, 75
Davis D. S., Richer H., Rich R., Reitzel D., Kalirai J., 2009, ApJ, 705, 398
Deal M., Deheuvels S., Vauclair G., Vauclair S., Wachlin F. C., 2013, A&A, 557, L12
Debes J. H., López-Morales M., 2008, ApJ, 677, L43
Debes J. H., Walsh K. J., Stark C., 2012, ApJ, 747, 148
Denissenkov P. A., 2010, ApJ, 723, 563
Dohnanyi J. S., 1969, J. Geophys. Res., 74, 2531
Dong R., Wang Y., Lin D. N. C., Liu X.-W., 2010, ApJ, 715, 1036
Dufour P. et al., 2007, ApJ, 663, 1291
Dupuis J., Fontaine G., Pelletier C., Wosemael F., 1992, ApJS, 82, 505
Dupuis J., Fontaine G., Pelletier C., Wosemael F., 1993a, ApJS, 84, 73
Dupuis J., Fontaine G., Wosemael F., 1993b, ApJS, 87, 345
Durda D. D., Greenberg R., Jedicke R., 1998, Icarus, 135, 431
Falcon R. E., Winget D. E., Montgomery M. H., Williams K. A., 2010, ApJ, 712, 585
Farihi J., Jura M., Zuckerman B., 2009, ApJ, 694, 805

Downloaded from https://academic.oup.com/mnras/article/439/4/3371/1151716 by guest on 24 March 2022

Farihi J., Barstow M. A., Redfield S., Dufour P., Hambly N. C., 2010, MNRAS, 404, 2123
Farihi J., Gänsicke B. T., Steele P. R., Girven J., Burleigh M. R., Breedt E., Koester D., 2012a, MNRAS, 421, 1635
Farihi J., Gänsicke B. T., Wyatt M. C., Girven J., Pringle J. E., King A. R., 2012b, MNRAS, 424, 464
Feigelson E. D., Nelson P. I., 1985, ApJ, 293, 192
Gänsicke B. T., Marsh T. R., Southworth J., Rebassa-Mansergas A., 2006, Science, 314, 1908
Gänsicke B. T., Koester D., Farihi J., Girven J., Parsons S. G., Breedt E., 2012, MNRAS, 424, 333
Garaud P., 2011, ApJ, 728, L30
Gehrels N., 1986, ApJ, 303, 336
Gilbert E. N., Pollack H. O., 1960, Bell Syst. Tech. J., 39, 333
Girven J., Brinkworth C. S., Farihi J., Gänsicke B. T., Hoard D. W., Marsh T. R., Koester D., 2012, ApJ, 749, 154
Graham J. R., Matthews K., Neugebauer G., Soifer B. T., 1990, ApJ, 357, 216
Greenstein J. L., 1974, AJ, 79, 964
Gubner J. A., 1996, SIAM J. Sci. Comput., 17, 750
Heng K., Tremaine S., 2010, MNRAS, 401, 867
Hoard D. W., Debes J. H., Wachter S., Leisawitz D. T., Cohen M., 2013, ApJ, 770, 21
Johnson J. A. et al., 2011, ApJS, 197, 26
Jura M., 2003, ApJ, 584, L91
Jura M., 2008, AJ, 135, 1785
Kenyon S. J., Bromley B. C., 2004, AJ, 127, 513
Klein B., Jura M., Koester D., Zuckerman B., Melis C., 2010, ApJ, 709, 950
Kleinman S. J. et al., 2013, ApJS, 204, 5
Koester D., 2009, A&A, 498, 517
Koester D., Wilken D., 2006, A&A, 453, 1051
Koester D., Provencal J., Shipman H. L., 1997, A&A, 320, L57
Koester D., Rollenhagen K., Napiwotzki R., Voss B., Christlieb N., Homeier D., Reimers D., 2005, A&A, 432, 1025
Koester D., Girven J., Gänsicke B. T., Dufour P., 2011, A&A, 530, A114
Krasinsky G. A., Pitjeva E. V., Vasilyev M. V., Yagudina E. I., 2002, Icarus, 158, 98
Kunze E., 2003, Prog. Oceanogr., 56, 399
Löhne T., Krivov A. V., Rodmann J., 2008, ApJ, 673, 1123
Lowen S. B., 1990, IEEE Trans. Inf. Theory, 36, 1302
Marois C., Macintosh B., Barman T., Zuckerman B., Song I., Patience J., Lafrenière D., Doyon R., 2008, Science, 322, 1348
Melis C. et al., 2012, ApJ, 751, L4
Metzger B. D., Rafikov R. R., Bochkarev K. V., 2012, MNRAS, 423, 505
Mohanty S. et al., 2013, ApJ, 773, 168
Montgomery M. H., Thompson S. E., von Hippel T., 2008, ApJ, 685, L133
O'Brien D. P., Greenberg R., 2003, Icarus, 164, 334
Paquette C., Pelletier C., Fontaine F., Michaud G., 1986, ApJS, 61, 197
Press W. H., Teukolsky S. A., Vetterling W. T., Flannery B. P., 2007, Numerical Recipes: The Art of Scientific Computing. Cambridge Univ. Press, New York
Rafikov R. R., 2011a, MNRAS, 416, L55
Rafikov R. R., 2011b, ApJ, 732, L3
Reach W. T., Kuchner M. J., von Hippel T., Burrows A., Mullally F., Kilic M., Winget D. E., 2005, ApJ, 635, L161
Reach W. T., Lisse C., von Hippel T., Mullally F., 2009, ApJ, 693, 697
Rice S. O., 1944, Bell Syst. Tech. J., 23, 282
Stancliffe R. J., Glebeek E., 2008, MNRAS, 389, 1828
Su K. Y. L. et al., 2007, ApJ, 657, L41
Traxler A., Garaud P., Stellmach S., 2011, ApJ, 728, L29
Udry S., Santos N. C., 2007, ARA&A, 45, 397
van Maanen A., 1917, PASP, 29, 258
Vauclair S., 2004, ApJ, 605, 874
Veras D., Mustill A. J., Bonsor A., Wyatt M. C., 2013, MNRAS, 431, 1686
von Hippel T., Thompson S. E., 2007, ApJ, 661, 477
Vitense Ch., Krivov A. V., Löhne T., 2010, A&A, 520, A32
Wyatt M. C., 2008, ARA&A, 46, 339
Wyatt M. C., Dent W. R. F., 2002, MNRAS, 334, 589
Wyatt M. C., Clarke C. J., Booth M., 2011, Celest. Mech. Dyn. Astron., 111, 1
Wyatt M. C., Smith R., Su K. Y. L., Rieke G. H., Greaves J. S., Beichman C. A., Bryden G., 2007, ApJ, 663, 365
Zuckerman B., Becklin E. E., 1987, Nature, 330, 138
Zuckerman B., Koester D., Reid I. N., Hünsch M., 2003, ApJ, 596, 477
Zuckerman B., Koester D., Melis C., Hansen B. M., Jura M., 2007, ApJ, 671, 872
Zuckerman B., Melis C., Klein B., Koester D., Jura M., 2010, ApJ, 722, 725

APPENDIX A: APPLICATION OF SHOT NOISE TO ACCRETION ON TO WHITE DWARFS

We are interested in computing the distribution of the mass of material still in the white dwarf atmosphere, $M_{\rm atm}$, as a result of the accretion of a succession of planetesimals, each of mass $m_{\rm p}$, given that the mass in the atmosphere drains exponentially on a time-scale $t_{\rm sink}$. This problem is analogous to various other problems in the current literature including dam theory (where dams are assumed filled by rainfall occurring stochastically), fluid queuing theory (which differs from ordinary queuing theory in that the number of customers in the queue can now be any real number and not just an integer) and risk theory in the computation of insurance claims. The origins of these theories date back to the late 19th century where considerations of shot noise in electrical systems began.

What interests us here is the computation of the distribution of the amplitude of shot noise, $I(t)$, caused by a superposition of impulses occurring at random Poisson distributed times $\ldots, t_{-1}, t_0, t_1, t_2, \ldots$, for the case in which all the impulses have the same shape, $F(t)$. In this case

$$I(t) = \sum_i F(t - t_i), \tag{A1}$$

and for the problem of interest to us

$$F(t) = H(t)\mathrm{e}^{-t}, \tag{A2}$$

where $H(t)$ is the Heaviside step function.

Gilbert & Pollak (1960) show that for the general case, the cumulative amplitude distribution function

$$Q(I) = Pr[I(t) \leq I] \tag{A3}$$

obeys an integral equation

$$I\,Q(I) = \int_{-\infty}^{I} Q(x)\,\mathrm{d}x + n\int_{-\infty}^{\infty} Q[I - F(t)]\,F(t)\,\mathrm{d}t, \tag{A4}$$

where n is the mean rate of arrival of shots.

For exponential shots, given by equation (A2), this can be written as a difference differential equation for density $P(I) = \mathrm{d}Q/\mathrm{d}I$, *viz.*

$$I\frac{\mathrm{d}P}{\mathrm{d}I} = (n-1)P(I) - nP(I-1), \tag{A5}$$

with the convention that $P(I) = 0$ when $I < 0$.

They show that for $0 < I < 1$,

$$P(I) = \frac{\mathrm{e}^{-n\gamma}}{\Gamma(n)}I^{n-1}, \tag{A6}$$

where $\gamma = 0.577\,215\,665\ldots$ is Euler's constant, and that for $I > 1$ the difference differential equation can be converted to an integral form

$$P(I) = I^{n-1}\left[\frac{\mathrm{e}^{-n\gamma}}{\Gamma(n)} - n\int_1^I P(x-1)\,x^{-n}\,\mathrm{d}x\right]. \tag{A7}$$

Downloaded from https://academic.oup.com/mnras/article/439/4/3371/1151716 by guest on 24 March 2022

Although for general shot functions, $F(t)$, the computation of the distribution function can be problematic (see, for example, Lowen 1990 and Gubner 1996), the numerical computation of $P(I)$ in this case is straightforward, as long as care is taken with the integrable singularity at $I = 0$ for $0 < n < 1$, that is, when the mean interval between shot is greater than the exponential decay time-scale.

For large values of $n, n \gg 1$, that is when a large number of shots occur during each decay time-scale, one can make use of the asymptotic formulation known as Campbell's theorem (Campbell 1909a,b). Campbell's Theorem states that for $n \gg 1$, the distribution asymptotically approaches that of a Gaussian or normal distribution with mean

$$\overline{I} = n \int_{-\infty}^{\infty} F(t)\,\mathrm{d}t, \tag{A8}$$

and standard deviation, σ, given by

$$\sigma^2 = n \int_{-\infty}^{\infty} [F(t)]^2\,\mathrm{d}t, \tag{A9}$$

with error of the order of $1/n$.

Rice (1944) has generalized Cambpell's theorem to the case when the shots have a distribution of amplitudes, which corresponds in our problem to the case when there is a distribution of asteroid masses. In this case, the amplitude $I(t)$ in equation A1 becomes

$$I(t) = \sum_i a_i F(t - t_i), \tag{A10}$$

where $\ldots\ a_1, a_2, a_3, \ldots$ are independent random variables all having the same distribution.

In this case, for $n \gg 1$ the distribution approaches that of a Gaussian or normal distribution with mean

$$\overline{I} = n\,\overline{a} \int_{-\infty}^{\infty} F(t)\,\mathrm{d}t, \tag{A11}$$

and standard deviation, σ, given by

$$\sigma^2 = n\,\overline{a^2} \int_{-\infty}^{\infty} [F(t)]^2\,\mathrm{d}t. \tag{A12}$$

This paper has been typeset from a TEX/LATEX file prepared by the author.

Downloaded from https://academic.oup.com/mnras/article/439/4/3371/1151716 by guest on 24 March 2022